(4)

The University of Texas at Dallas
Center for Quantum Electronics
The Gamma-Ray Laser Project
Quarterly Report
April-June 1989

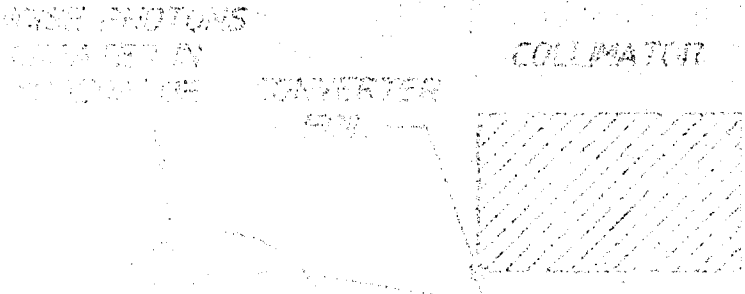

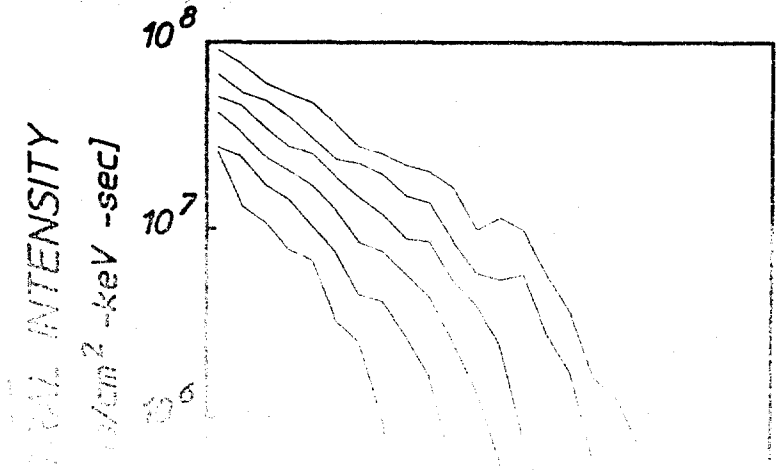

Report GRL/8901

PROOF OF THE FEASIBILITY OF COHERENT AND INCOHERENT SCHEMES FOR PUMPING A GAMMA-RAY LASER

Principal Investigator: Carl B. Collins
The University of Texas at Dallas
Center for Quantum Electronics
P.O. Box 830688
Richardson, Texas 75083-0688

July 1989

Quarterly Technical Progress Report
1 April 1989 through 30 June 1989
Contract Number N00014-86-C-2488

Prepared for
INNOVATIVE SCIENCE AND TECHNOLOGY DIRECTORATE
OF STRATEGIC DEFENSE INITIATIVE ORGANIZATION

Contracting Officer's Technical Representative
Dr. Paul Kepple, Code 4720
Naval Research Laboratory
4555 Overlook Avenue, SW
Washington, DC 20375-5000

SECURITY CLASSIFICATION OF THIS PAGE (When Data Entered)

REPORT DOCUMENTATION PAGE		READ INSTRUCTIONS BEFORE COMPLETING FORM
1. REPORT NUMBER GRL/8901	2. GOVT ACCESSION NO.	3. RECIPIENT'S CATALOG NUMBER
4. TITLE (and Subtitle) PROOF OF THE FEASIBILITY OF COHERENT AND INCOHERENT SCHEMES FOR PUMPING A GAMMA-RAY LASER		5. TYPE OF REPORT & PERIOD COVERED Quarterly Technical Progress 04/01/89 - 06/30/89 6. PERFORMING ORG. REPORT NUMBER
7. AUTHOR(s) C. B. Collins		8. CONTRACT OR GRANT NUMBER(s) N00014-86-C-2488
9. PERFORMING ORGANIZATION NAME AND ADDRESS University of Texas at Dallas Center for Quantum Electronics P.O. Box 830688 Richardson, TX 75083-0688		10. PROGRAM ELEMENT, PROJECT, TASK AREA & WORK UNIT NUMBERS
11. CONTROLLING OFFICE NAME AND ADDRESS INNOVATIVE SCIENCE AND TECHNOLOGY DIRECTORATE OF STRATEGIC DEFENSE INITIATIVE ORGANIZATION		12. REPORT DATE July 1989 13. NUMBER OF PAGES 61
14. MONITORING AGENCY NAME & ADDRESS(if different from Controlling Office) Dr. Paul Kepple Naval Research Laboratory, Code 4720 4555 Overlook Avenue, SW Washington, DC 20375-5000		15. SECURITY CLASS. (of this report) Unclassified 15a. DECLASSIFICATION/DOWNGRADING SCHEDULE

16. DISTRIBUTION STATEMENT (of this Report)

This document has been approved for public release and sale; its distribution is unlimited.

17. DISTRIBUTION STATEMENT (of the abstract entered in Block 20, if different from Report)

18. SUPPLEMENTARY NOTES

19. KEY WORDS (Continue on reverse side if necessary and identify by block number)

20. ABSTRACT (Continue on reverse side if necessary and identify by block number)

Recent approaches to the problem of the gamma-ray laser have focused upon upconversion techniques in which metastable nuclei are pumped with long wavelength radiation. At the nuclear level the storage of energy can approach tera-Joules (10^{12}J) per liter for thousands of years. However, any plan to use such a resource for a gamma-ray laser poses problems of a broad interdisciplinary nature requiring the fusion of concepts taken from relatively unrelated fields of physics. Our research group has described several means through which this energy
(continued on next page)

DD FORM 1 JAN 73 1473 EDITION OF 1 NOV 65 IS OBSOLETE
S/N 0102-LF-014-6601

SECURITY CLASSIFICATION OF THIS PAGE (When Data Entered)

20. Abstract (continued)

might be coupled to the radiation fields with cross sections for stimulated emission that could reach 10^{-17} cm^2. Such a stimulated release could lead to output powers as great as 3×10^{21} Watts/liter. Since 1978 we have pursued an approach for the upconversion of longer wavelength radiation incident upon isomeric nuclear populations that can avoid many of the difficulties encountered with traditional concepts of single photon pumping. Recent experiments have confirmed the general theory and have indicated that a gamma-ray laser is feasible if the right combination of energy levels and branching ratios exists in some real material. Of the 1,886 distinguishable nuclear materials, the present state-of-the-art has been adequate to identify 29 first-class candidates, but further evaluation cannot proceed without remeasurements of nuclear properties with higher precision. A laser-grade database of nuclear properties does not yet exist, but the techniques for constructing one have been developed under this contract and are now being utilized. Resolution of the question of the feasibility of a gamma-ray laser now rests upon the determination of: 1) the identity of the best candidate, 2) the threshold level of laser output, and 3) the upconversion driver for that material.

This quarter's report focuses upon two of the new technologies we have developed to aid in the demonstration of the feasibility of a gamma-ray laser. Benefiting from the scientific momentum already realized along the approach to incoherent pumping, they have continued to advance the nuclear analog of the ruby laser. There have been embodied the very simplest of the concepts for a gamma-ray laser and it is no surprise that the greatest rate of achievement has continued in that direction. One powerful technology spun-off last year was the method for X-ray Activation of Nuclei (XAN) to calibrate intense bremsstrahlung sources operating in the range 0.2 to 1.4 MeV. Now, results of studies of the photoactivation of nuclear isomers with DNA/AURORA seem to show that the XAN methodology could be extended for the calibration of intense bremsstrahlung sources, even to 12 MeV -- well above the threshold for the evaporation of neutrons from both target and environmental materials. Unlike previous experiments conducted below 6 MeV in which there was no significant generation of spurious neutrons, in these high energy tests there was the expected production of neutrons. These photoneutron fluxes were calibrated and target packages were designed so that some isotopes could still be used for (γ,γ') experiments. In those cases the photoexcitation reactions for the production of isomers could be isolated without serious interference from neutron contributions. This ability to separate some selective reactions for (γ,γ') activation points the way for an extension of the XAN methodology over the range of photon energies reaching 12 MeV.

As has been the case at lower energies, success in calibrating a selection of targets for use in XAN is dependent upon access to a bremsstrahlung source with a variable endpoint. Fewer than five such facilities exist anywhere and access is not yet assured to any one of them. In contrast, there is a considerable availability of fixed endpoint machines of the type used in medical radiation therapy. The final section of this report focuses upon the extent to which such a fixed energy linac could be adapted for use as a source of variable endpoint bremsstrahlung. Preliminary results are promising and prospects are encouraging that the XAN procedure can be extended for use in calibrating x-ray pump sources over an extended range of photon energies.

TABLE OF CONTENTS

PREFACE

This report focuses upon some of the exciting new technologies which have matured during the current reporting period. These advances are making it possible to pursue our fundamental research into the feasibility of a gamma-ray laser with even greater intensity. Benefiting from the scientific momentum already realized along the approach to incoherent pumping, most have continued to advance the nuclear analog of the ruby laser. There have been embodied the very simplest of the concepts for a gamma-ray laser and it is no surprise that the greatest rate of achievement has continued in that direction.

One powerful technology spun-off last year was the method for X-ray Activation of Nuclei (XAN) to calibrate intense bremsstrahlung sources operating in the range 0.2 to 1.4 MeV. As now implemented, five isotopes, ^{77}Se, ^{79}Br, ^{111}Cd, ^{115}In, and ^{167}Er are used to sample narrow spectral slices of the bremsstrahlung fluence illuminating a target. The isotopes are excited to long-lived states whose nuclear fluorescences can be "read-out" at a later time at which there is less electrical noise. With five isotopes the XAN method accommodates measurement at five photon energies in the range 0.2 to 1.4 MeV. More recently it has been shown that opportunities exist for the standardization of a selection of isotopes in order to extend the capabilities for this type of calibration. Structure observed in the photoexcitation of 19 isomers has suggested that it will be possible to span the range from 1.4 to 6.0 MeV which is of interest in medical radiation therapy.

Receiving first emphasis this quarter are the surprising results of studies of the photoactivation of nuclear isomers with DNA/AURORA. These seem to show that the XAN methodology could be extended for the calibration of intense bremsstrahlung sources, even to 12 MeV -- well above the threshold for the evaporation of neutrons from both target and environmental materials. *Unlike previous experiments conducted below 6 MeV in which there was no significant generation of spurious neutrons*, in these high energy tests there was the expected production of neutrons. These photoneutron fluxes were calibrated and target packages were designed so that some isotopes could still be used for (γ,γ') experiments. In those cases the photoexcitation reactions for the production of isomers could be isolated without serious interference from neutron contributions. This ability to separate some selective reactions for (γ,γ') activation points the way for an extension of the XAN methodology over the range of photon energies reaching 12 MeV.

As was shown in our early work with DNA/PITHON, success in calibrating a selection of targets for use in XAN is dependent upon access to a bremsstrahlung source with a variable endpoint. Fewer than five such facilities exist anywhere and access is not yet assured to any one of them. In contrast, there is a considerable availability of fixed endpoint machines of the type used in medical radiation therapy. The final section of this report focuses upon the extent to which such a linac could be adapted for use as a source of variable endpoint bremsstrahlung. As can be seen, preliminary results are promising and prospects are encouraging that the XAN procedure can be extended for use in calibrating x-ray pump sources over an extended range of photon energies.

As has been the case since 1982, there are still no known factors which inhibit the realization of a gamma-ray laser. Neither the level of pump fluence required for laser threshold nor the waste heat to reject presents any particular problem in idealized materials. *A gamma-ray laser is feasible if the right combination of energy levels occurs in some real material.* When actually tested, the two poorest of the 29 candidate nuclei did surprisingly well, performing 1,000 to 10,000 times better than expected. The overriding question in resolving the feasibility of the nuclear analog to the ruby laser is whether or not one of the better of the 29 has its isomeric level in a position sufficiently near the ideal.

Continuing the preparation of this report as an "in-house" journal, this series presents material to reflect the individual contributions of the teams of research faculty and graduate students involved in these phases of the research. In this regard, I wish to thank all our staff for their splendid efforts in supporting the preparation of these manuscripts to a rather demanding timetable.

- C. B. Collins
- Director
- Center for Quantum Electronics

N00014-86-C-2488
UTD #24522-964

PHOTOEXCITATION OF NUCLEAR ISOMERS WITH THE DNA/AURORA NUCLEAR SIMULATOR

by J. J. Carroll, J. A. Anderson, M. J. Byrd, K. N. Taylor, D. G. Richmond, T. W. Sinor and C. B. Collins

Center for Quantum Electronics, University of Texas at Dallas

Introduction

The DNA/Aurora nuclear simulator at the Harry Diamond Laboratories is the largest flash x-ray accelerator in the world.[1] Since 1971 the simulator has proved to be an indispensable tool in the laboratory testing of devices for their hardness to radiation from a nuclear explosion. In addition to bremsstrahlung with endpoint energies approaching 11 MeV, the machine has acquired the capability of producing a softened x-ray environment[2] with large dose-area products by Compton scattering of the photons from a material with low Z. Electron beams may also be used for direct irradiation of targets or for the production of intense microwave radiation.[3]

The accelerator proper consists of a 5 MJ Marx generator which drives four parallel oil-filled coaxial Blumleins. Each Blumlein connects to a vacuum transmission line terminating in a diode, and bremsstrahlung is produced by placing a converter target of suitable material at the cathode. The use of all four transmission lines provides a dose-area product of about 240 Gy-m^2. This corresponds to a dose of 400 Gy (40 kRad) in a volume of about 0.1 m^3 centered near the intersection point of the transmission line axes, called the "hot spot".[4] The endpoint energy of the photon spectrum may be varied while maintaining a high delivered dose by altering several machine parameters, notably the charge voltage of the Marx bank. For the purposes of the current investigation this is an important feature of the machine since the DNA/Aurora nuclear simulator can therefore be used to examine an additional class of physical phenomena, that of the photoexcitation of nuclear isomers.

The photoexcitation of isomeric nuclei through (γ,γ') reactions has been investigated for more than fifty years.[5,6] However, until this past year there has been very little convergence among the few tens of experimental results that have been published in the literature.[7] The extreme variance between earlier measurements is surprising when compared with the precision routinely achieved in the examination of all types of particle reactions. Moreover, the analogous optical double resonance technique is among the most powerful methods of investigation at the molecular level. Nevertheless, (γ,γ') studies have traditionally provided widely differing results.

It is generally thought that (γ,γ') reactions occur through resonant absorption processes. However, in an attempt to explain the seemingly excess activations observed in some experiments, several investigators[8,9] have postulated that the photoexcitation proceeds instead through a non-resonant channel even at energies below 1.5 MeV. Theory has never been able to supply a mechanism of sufficient magnitude to justify this suggestion at such relatively low energies, but the idea remained a controversial[7] alternative to resonant excitation for some time.

In 1987 the technology became available[10,11] to directly measure the spectrum of a variable energy source of pulsed bremsstrahlung in the 0.5 to 1.5 MeV range. Using such a device, the DNA/PITHON nuclear simulator at Physics International,[12,13] it was found that in the cases of $^{115}In^{m}$ and $^{111}Cd^{m}$ the isomeric states were excited by predominantly resonant absorption through intermediate states, called gateway states. These states were near 1 MeV and were broadened by their relatively short lifetimes. The sharp onset of the (γ,γ') reactions with increasing energy relegated to less than 3% any contributions from non-resonant processes and indicated that the gateway states were reasonably well connected by radiative transitions to both the ground states and the isomers. It appears therefore that the principal cause for the large discrepancy between previous measurements was the difficulty in adequately characterizing the spectra of the irradiating sources rather than the appearance of true non-resonant absorption.

The identification of relatively narrow gateway states below 1.5 MeV for the photoexcitation of isomers and the measurement of integrated cross sections for activation through these levels has reopened the question of the existence of similar gateways in the region from 1.5 to

6 MeV. In this energy range very early data[14,15] indicated that yields from (γ,γ') reactions increased as mediating states were accessed at higher energies. Evidence was accumulated in the form of increases in the slopes of curves showing isomeric yields as functions of the endpoint energies of the bremsstrahlung used to pump the reactions, but the changes were not dramatic. The largest integrated cross section found[15] was $(380 + 200 - 100) \times 10^{-29}$ cm^2-keV for the photoexcitation of $^{87}Sr^m$ through a gateway at 2.66 MeV.

Recently a renaissance in the study of (γ,γ') reactions was launched by the availability of medical linear accelerators which can serve as intense and stable bremsstrahlung sources. The total doses which these devices can deposit in reasonable working periods have made possible the examination of reactions involving even rare nuclides for which target masses are limited to milligrams. In this way, the first (γ,γ') reaction leading to the deexcitation of an isomeric sample, $^{180}Ta^m(\gamma,\gamma')^{180}Ta$, was studied[16] with unexpected results.

The isomer $^{180}Ta^m$ is nature's rarest naturally occurring isotope.[17] Requiring an unlikely change of $\Delta J = 8$, the isomer was dumped to the ground state by bremsstrahlung having an endpoint energy of about 6 MeV. The partial width for this reaction was found[16] to be at least 0.5 eV, an enormous value exceeding any previous reports for (γ,γ') reactions by two to three orders of magnitude. The amount of deexcitation observed for the isomer was astonishing, corresponding to a total integrated cross section in excess of 7×10^{-25} cm^2-keV. This strength of the dumping reaction was qualitatively confirmed[18] with bremsstrahlung from the injector to the Darmstadt superconducting electron machine operated at 4.6 MeV. Even more recent experiments[19] have shown that the strength of this reaction is only slightly diminished below 4 MeV, giving a total integrated cross section of about 1.6×10^{-25} cm^2-keV.

The fact that the endpoint energies of the medical linacs cannot be continuously tuned prevents the duplication of the kind of detailed successes achieved below 1.5 MeV with the variable endpoint DNA/PITHON machine. Nevertheless, experimental results obtained from samples irradiated with this type of x-ray source have formed a foundation for further investigations which might provide better resolution. These studies,[19] which used 4 and 6 MeV fixed endpoint medical linacs, support the position that in most cases resonant processes are still dominant up to energies of about 6 MeV. However, the question of possible non-reso-

nant absorption by isomeric nuclei at energies near their neutron evaporation thresholds remains to be answered conclusively.

The DNA/Aurora nuclear simulator allows the further examination of resonant vs. non-resonant photoexcitation in the energy range of 6 to 11 MeV. It also provides inferential information about the photoactivation process below 6 MeV. Moreover, preliminary analysis indicates that resonant excitation of nuclei continues to be important throughout the range of energies accessed by DNA/Aurora.

Analytic and Experimental Methods

The number of isomeric nuclei excited through a (γ,γ') reaction, $N_{excited}$, is given by

$$N_{excited} = N_T \int_0^{E_{end}} \sigma(E) \left[\frac{d\Phi(E)}{dE} \right] dE, \qquad (1)$$

where $\sigma(E)$ is the reaction cross section, $d\Phi(E)/dE$ is the photon spectral intensity of the pump source in photons/cm^2-keV, N_T is the number of target nuclei and E_{end} is the endpoint energy of the irradiating bremsstrahlung. The spectral intensity can be expressed as the product of the total photon flux Φ_o and a relative spectral intensity function F(E). The combination $N_{excited}/N_T$ is commonly referred to as the activation.

Equation 1 may be simplified for (γ,γ') reactions proceeding through resonant gateways which are narrow relative to any structure of the irradiating source spectrum. In this case, as the experiments below 1.5 MeV demonstrated, Equation 1 becomes

$$N_{excited} = N_T \sum_i (\sigma\Gamma)_i \left[\frac{d\Phi(E_i)}{dE} \right]. \qquad (2)$$

Here $d\Phi(E_i)/dE$ is the photon intensity at the gateway energy E_i and Γ_i is the natural width in keV of the i^{th} mediating state. From the uncertainty principle, $\Gamma_i \geq \hbar/\tau_i$, where τ_i is the lifetime of the state.

The quantity $(\sigma\Gamma)_i$ is the integrated cross section given in the usual units of 10^{-29} cm^2-keV and is defined by

$$(\sigma\Gamma)_i = \int_{i^{th}\ \text{resonance}} \sigma(E)\, dE. \qquad (3)$$

This is often expressed as $\pi b_a b_o \sigma_o \Gamma/2$ where b_a and b_o are the branching ratios for decay from the gateway level to the ground and isomeric states. The product $b_a b_o \Gamma$ is called the partial width for the transition. The quantity σ_o is the amplitude of the Breit-Wigner cross section for the absorption transition,

$$\sigma_o = \frac{\lambda^2}{2\pi} \frac{I_e + 1}{I_g + 1} \frac{1}{\alpha_p + 1}, \qquad (4)$$

where λ is the wavelength of the γ-ray at the resonant energy, I_e and I_g are the nuclear spins of the excited and ground states, and α_p is the internal conversion coefficient for the absorption transition.

The current experiments examine the activations of sample nuclei in the context of this formalism as functions of the Marx bank charge voltage which reflects the endpoint energy of the irradiating bremsstrahlung. The appearance of any sharp increases or steps in the data therefore indicates the excitation of a resonant gateway and allows the estimation of the integrated cross section for the state according to Equation 2. It is also instructive to calculate the integrated cross section of a single, hypothetical gateway that would produce all of the activation observed in the lower charge voltage irradiations. These values, given as a function of the assumed gateway energy, allow the results of the DNA/Aurora experiments to be compared with the previous 6 MeV linac studies which provided only this latter type of information. This was due to the limitations imposed by a fixed endpoint energy. The integrated cross section of a single dominant gateway state located at energy E is calculated from Equation 2 as

$$\sigma\Gamma(E) = \frac{N_{excited}}{N_T} \left[\frac{d\Phi(E)}{dE} \right]^{-1}. \qquad (5)$$

The irradiation of sample materials was accomplished by suspending the targets in the hot spot where complex sample packages were exposed

to a flash x-ray shot produced by a particular charge voltage. The experimental data base was built up by exposing many similar target packages to shots taken at different charge voltages. The individual sample materials were in the form of either metallic foils, as in the case of indium and cadmium, or in the form of metallic chips or chemical compounds held in plastic vials or cylindrical planchettes. Foils and planchettes were exposed with their faces normal to the machine centerline. The vials were exposed with their axes perpendicular to the machine centerline. All samples were backed with an array of Thermoluminescent Dosimeters, or TLD's, in order to accurately measure the dosage which each target received.

The materials irradiated in these experiments are listed in Table I. The short half-lives of some of the isomeric states to be excited made it necessary to use a pneumatic shuttle system to transport the vials, called rabbits, with these samples from the hot spot to a shielded, well-type NaI(Tl) spectrometer system located outside of the irradiation chamber. This detector was monitored by a personal computer which allowed the acquisition of spectra of both the energy and, when desirable, the time dependence of the observed fluorescence from the isomers. Moderately long-lived materials were transported to a detector by hand from within the target chamber following irradiation; foils and planchettes were counted with a solid NaI(Tl) detector system and vials were again studied with the well detector. Samples containing particularly long lived isomers such as $^{123}Te^{m}$, the longest-lived isomer successfully photoactivated[20] with $T_{1/2}$ = 119.7 days, and ^{117}Sn ($T_{1/2}$ = 13.61 days) were transported to the Center for Quantum Electronics where the samples were counted on a high-purity, n-type germanium spectrometer.

Table I

Summary of isomeric nuclei studied. In the sample column, R refers to samples contained in rabbits, P to flat planchettes, and F to metallic foils. The self-absorption corrections represent the fraction of fluorescent photons which reach the detector.

Nuclide	Abundance [%]	Sample Form	$T_{1/2}$	Principle Fluorescence [keV]	Self-Absorption Correction
^{167}Er	22.95	Er_2O_3 (R)	2.28 sec	207.79 (41.70%)	57.90
^{79}Br	50.69	LiBr (R)	4.86 sec	207.20 (75.80%)	84.90
^{89}Y	100.00	YF_3 (R)	16.06 sec	909.15 (99.14%)	94.70
^{77}Se	94.38	Se (R)	17.45 sec	161.92 (52.40%)	72.28
^{199}Hg	16.90	Hg_2Cl_2 (R)	43.20 sec	158.40 (53.00%)	43.96
^{137}Ba	11.74	BaF_2 (R)	2.55 min	661.66 (90.10%)	95.50
^{111}Cd	12.80	Cd (F)	48.6 min	245.49 (94.00%)	76.35
^{113}In	4.30	In (F)	1.66 hr	391.69 (64.20%)	98.30
^{87}Sr	7.00	SrF_2 (P)	2.81 hr	388.40 (82.30%)	95.78
^{115}In	95.70	In (F)	4.49 hr	336.26 (45.80%)	98.00
^{180}Ta	0.012	Ta (F)	8.15 hr	55.79 (36.00%)	54.77
^{135}Ba	6.60	BaF_2 (P)	1.20 d	268.27 (15.60%)	94.33
^{117}Sn	7.70	Sn (F)	13.6 d	158.56 (86.40%)	92.89

The isomeric activation present in each sample was obtained from the number of decays of the excited states observed in the counting intervals. This was reflected by the counts contained in the full energy peaks of the isomeric fluorescence lines in the energy spectra. The values were corrected for the finite duration of the counting period using literature values for the half-lives, measured detector efficiencies and the observed intensities of the fluorescence photons. While the target samples are essentially transparent to the pump photons, some self-absorption is possible at the lower fluorescence energies. The measurements were corrected for this self-absorption by a factor calculated by Monte-Carlo methods for each sample and detector geometry. These calculations were tested by comparing the values obtained from samples containing identical materials, but in different geometries. The activations of each isomer were normalized to the dose delivered to the samples and were examined as functions of charge voltage. The integrated cross sections necessary to produce the activation through a single gateway were determined from the activations by using bremsstrahlung spectra obtained from TIGER[21] code calculations performed by the Aurora facility.[22,23] Figure 1 shows the function F(E) of a typical 80 kV shot for which $\Phi_0 = 2.39 \times 10^{11}$ photons/cm^2-Gy. The discrete nature of the available spectra makes it necessary to consider the photon spectral intensity as the number of photons/cm^2 per energy bin width.

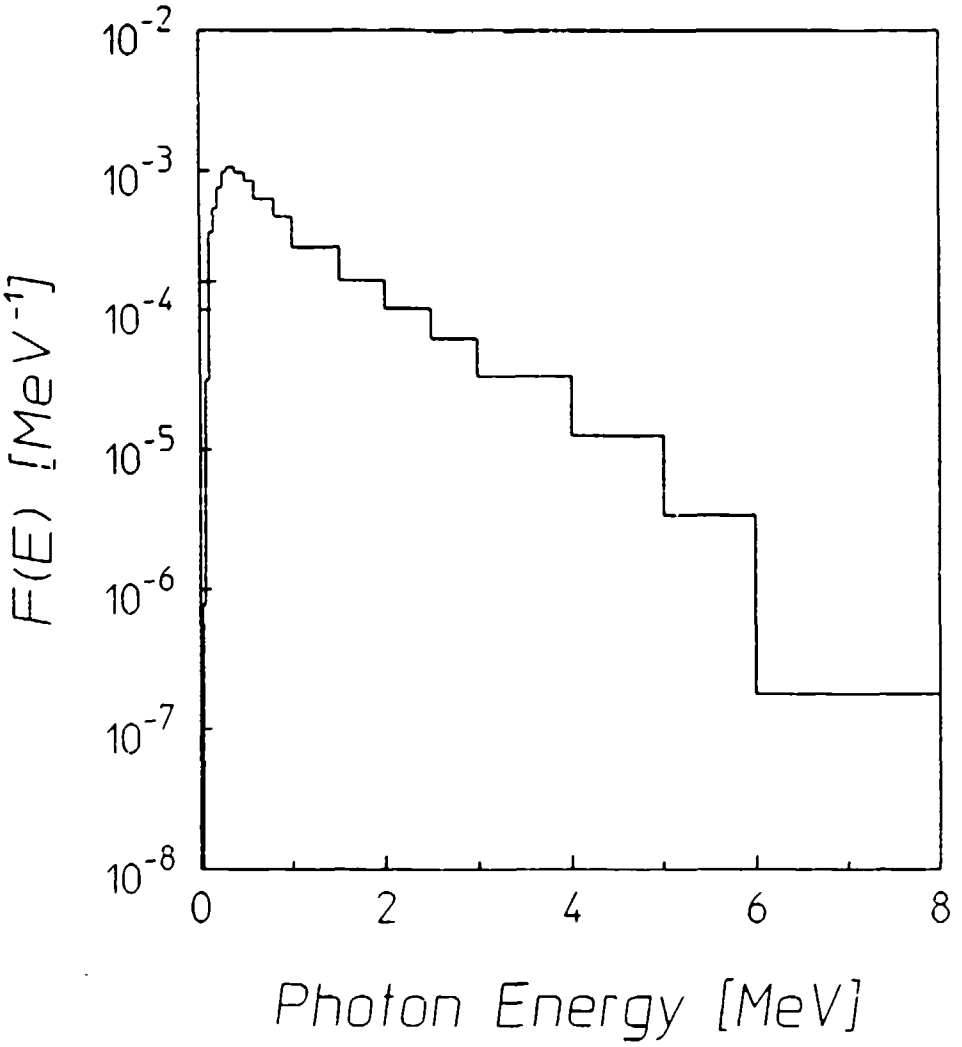

Figure 1: Relative spectral intensity function F(E) of the bremsstrahlung produced by DNA/Aurora charged to 80 kV. The function is normalized so that the integral under the curve is unity.

Results

An energy spectrum which was obtained from an indium sample following an 80 kV irradiation is shown in Figure 2. The significant amount of activation of the isomers $^{113}In^{m}$ and $^{115}In^{m}$ is indicated by their fluorescence lines at 391.69 keV and 336.26 keV, respectively. The full energy peaks are large enough to provide 5% counting statistics. The size and distinct appearances of the isomeric decay signatures in this spectrum is typical of measurements obtained from samples in which activation took place. The only instance in which a clear identification of the fluorescence peaks can not be made arises in the case of silver samples which contain both ^{107}Ag and ^{109}Ag nuclei. These samples showed strong activation, but the resolution of the NaI(Tl) spectrometer is insufficient to separate the contributions of the fluorescence lines at 93.146 keV for $^{107}Ag^{m}$ and 88.034 keV for $^{109}Ag^{m}$.

All of the isomeric nuclei irradiated with the DNA/Aurora accelerator were activated with the exception of the isomers of ^{190}Os, ^{192}Os and ^{90}Zr. Samples containing these nuclei showed no evidence of isomeric activation at even the highest charge voltage, 118 kV. The remaining target nuclei were successfully examined by the previously discussed approach with the result that most of the nuclides fall into two categories.

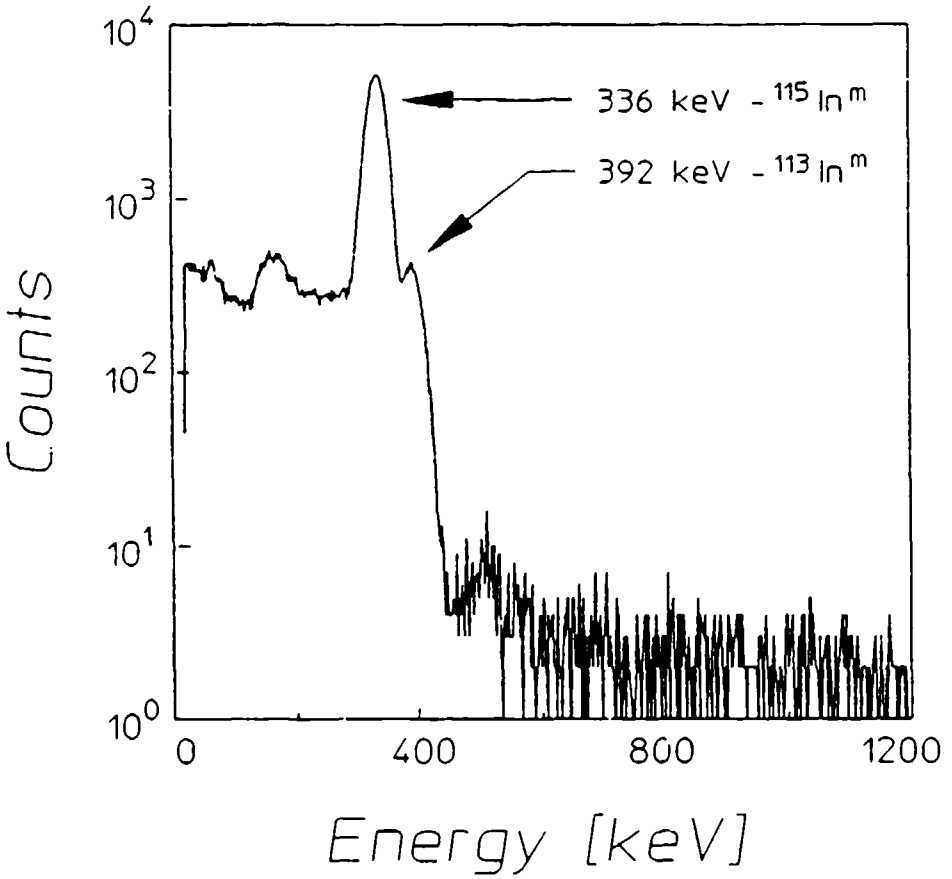

Figure 2: Pulse height spectrum showing the 336.26 keV fluorescence line from the decay of $^{115}In^m$ and the 391.69 keV line from the decay of $^{113}In^m$. The measurement was obtained with a 7.6 cm × 7.6 cm diameter solid NaI(Tl) detector. The counting period was 600 sec.

The first group contains two nuclei for which resonant absorption is apparent in the energy range scanned by DNA/Aurora. One such nuclide is ^{199}Hg. A plot of the normalized activation of the isomer as a function of charge voltage is shown in Figure 3. The step which appears in this plot reflects an increase in activation by a factor of 3.7 between 80 and 90 kV charges. This change is a radical departure from the rather slow rise in activation seen elsewhere in the figure where the activation grows by a factor of 0.06 for every 10 kV increase in charge voltage. Such a sharp jump can only be the result of a narrow gateway which is accessed by photons having energies greater than the endpoint energy of the bremsstrahlung from the 80 kV shots.

The integrated cross section of the gateway state in ^{199}Hg cannot be exactly calculated since the energy bin which contains the probable gateway location of 7 to 7.5 MeV is particularly wide, including all photons from 6 to 8 MeV. However, by subtracting the activation at 80 kV from that at 90 kV it is possible to estimate a residual value of 1.8×10^{-23} cm^2-keV. This compares with 2.6×10^{-25} cm^2-keV, the largest possible integrated cross section for states accessed by 6 MeV bremsstrahlung.[19] It is interesting to note that an 80 kV charge voltage corresponds roughly to a bremsstrahlung endpoint energy of between 7 and 7.5 MeV, while the neutron evaporation threshold energy for ^{199}Hg is 6.67 MeV.

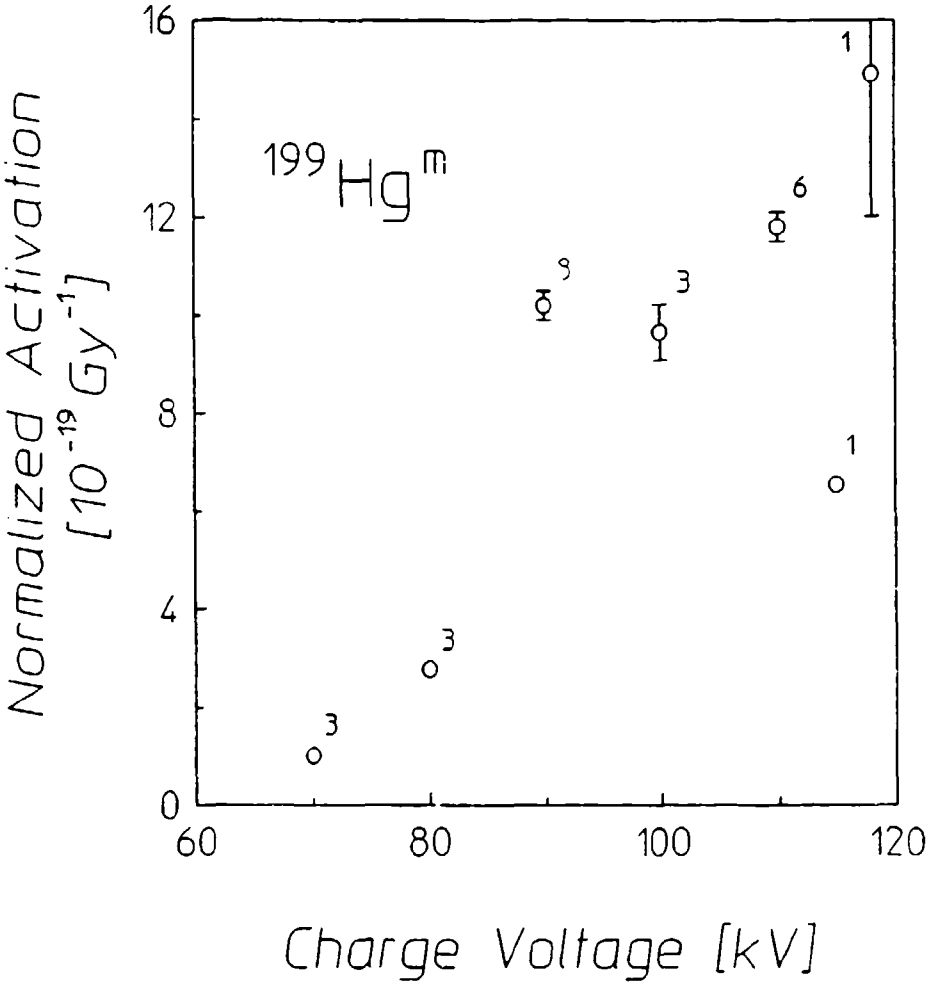

Figure 3: Activation observed in samples containing ^{199}Hg following exposure to DNA/Aurora shots taken at different charge voltages. These values are the result of multiple measurements as indicated by the numbers to the upper right of the data points. The activation has been normalized to the dosage delivered to the samples. The size of the symbols is comparable to one standard deviation where no error bars are shown.

The fact that a resonant excitation through (γ,γ') reactions appears so near, and in fact within, the single particle continuum is surprising but there are compelling reasons which support a confidence in this finding. Decay of the isomer $^{199}Hg^{m}$ produces two strong signature peaks located at 158.38 keV and 374.1 keV from the IT cascade, both of which were analyzed to determine the amount of activation. Also, as mentioned before, the results displayed in Figure 3 were obtained from multiple shots taken at the same charge voltage whenever possible. The number of measurements available for each charge is given in the figure to the immediate upper right of each of the points. Therefore there are few cases where the data can be questioned on statistical grounds. In Figure 3 only the points at 115 and 118 kV can be considered to be in doubt on this basis. Indeed, these high charge voltages lie at the upper limit which can be achieved with DNA/Aurora. Shots taken at these charges often suffer from prefiring of sections of the Marx bank. Therefore, there is a resulting uncertainty in the corresponding bremsstrahlung endpoint energies which is difficult to quantify. The size of the error bars is primarily due to variations in the determination of the delivered dose from the TLD's, not from the random error associated with the counting of decay events.

The strongest logical argument for the validity of these results is most clearly presented by examining Figure 4. This plot shows the integrated cross sections of single gateways as functions of assumed energy derived from the 6 MeV linac studies of reference 19 and those due to irradiations achieved with Aurora charged to 80 kV. This is the lowest charge voltage for which a photon spectrum is available. The values provided by the two experimental series are essentially the same between 2 MeV, the smallest energy at which a dominant mediating state could be expected to lie, and 6 MeV. The photoexcitation achieved with bremsstrahlung having an endpoint of about 7 MeV from DNA/Aurora therefore proceeded through the same channel accessed by the 6 MeV linac. This verifies that for this isotope the present experiments are consistent with the previous studies. It is difficult to suggest that all the higher charge voltage shots could be in error. It could be argued, however, that the 70 and 80 kV points are significantly too low and should agree more closely with the 90 to 110 kV shots. This still requires the existence of a resonant state above 6 MeV, as is apparent from Figure 4. In this case the integrated cross section from the

present studies would be much larger than that from the 6 MeV linac results, again indicating a previously unaccessed, narrow state.

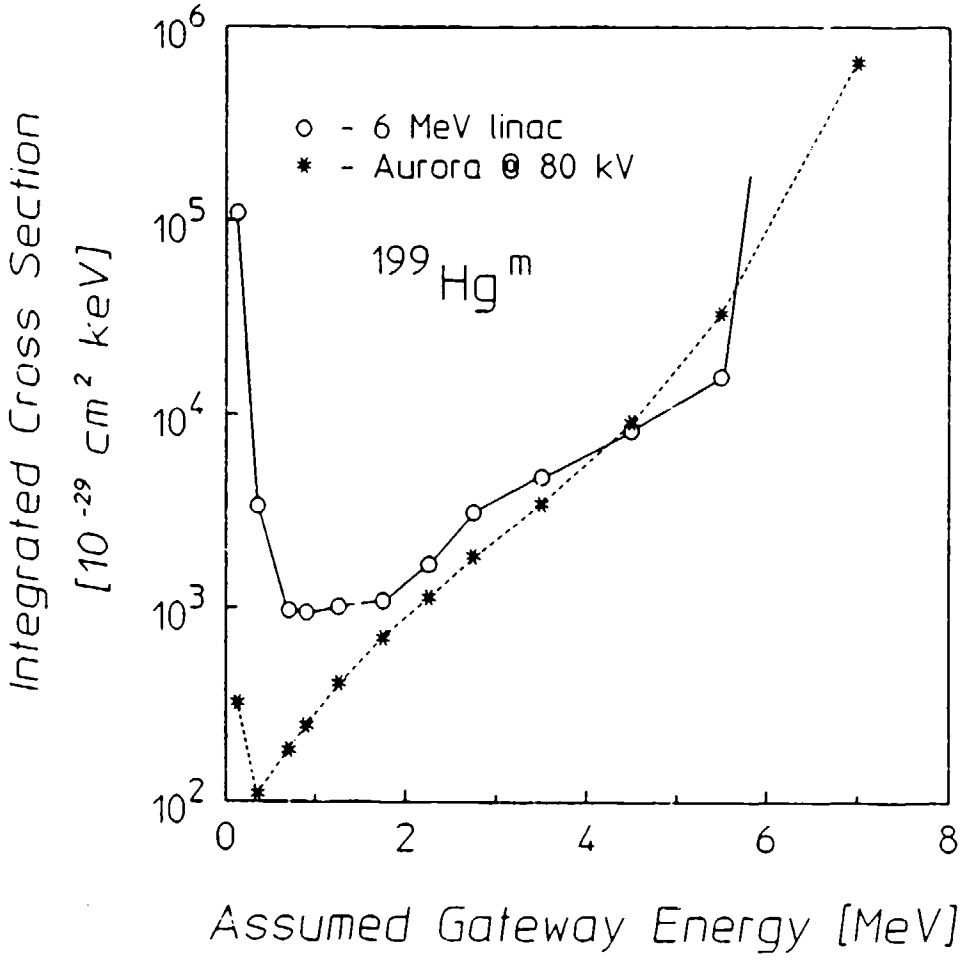

Figure 4: Integrated cross section for a single dominant resonance as a function of the energy at which it is assumed to lie. The circles indicate values derived from previous experimental studies performed with a 6 MeV endpoint linac. The asterisks show the results determined from the normalized activation produced by DNA/Aurora when charged to 80 kV.

The nucleus ^{111}Cd exhibits similar evidence of excitation through a gateway lying above 6 MeV. The normalized activation of this isomer as a function of charge voltage is shown in Figure 5. The plot clearly shows the presence of a jump in the data due to resonant absorption between 7 and 7.5 MeV, and again the lower energy activations correspond well with the results from the linac studies. This latter comparison is given in Figure 6. The residual integrated cross section for this state is 6.9×10^{-23} cm^2-keV, while the largest integrated cross section for a state below 6 MeV is 4.6×10^{-25} cm^2-keV. The photoneutron threshold for this isotope is 6.98 MeV.

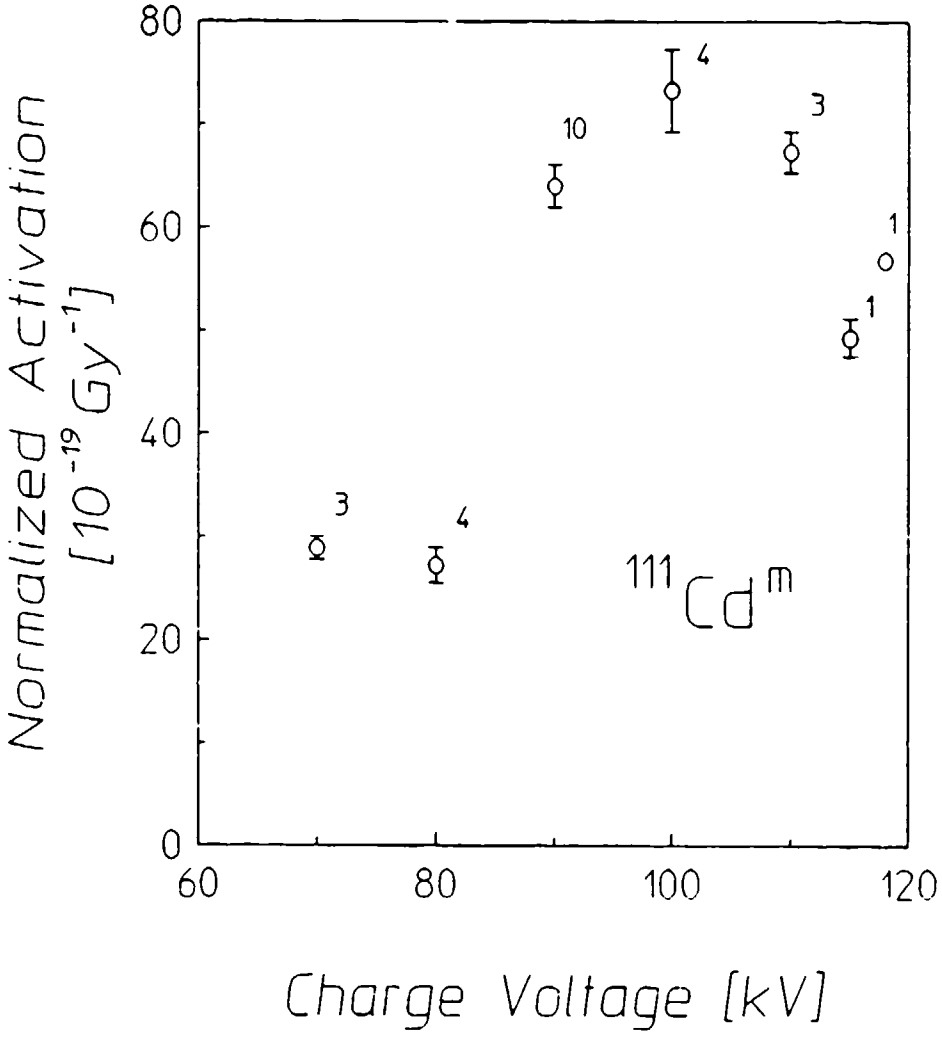

Figure 5: Activation observed in samples containing ^{111}Cd following exposure to DNA/Aurora shots taken at different charge voltages. These values are the result of multiple measurements as indicated by the numbers to the upper right of the data points. The activation has been normalized to the dosage delivered to the samples. The size of the symbols is comparable to one standard deviation where no error bars are shown.

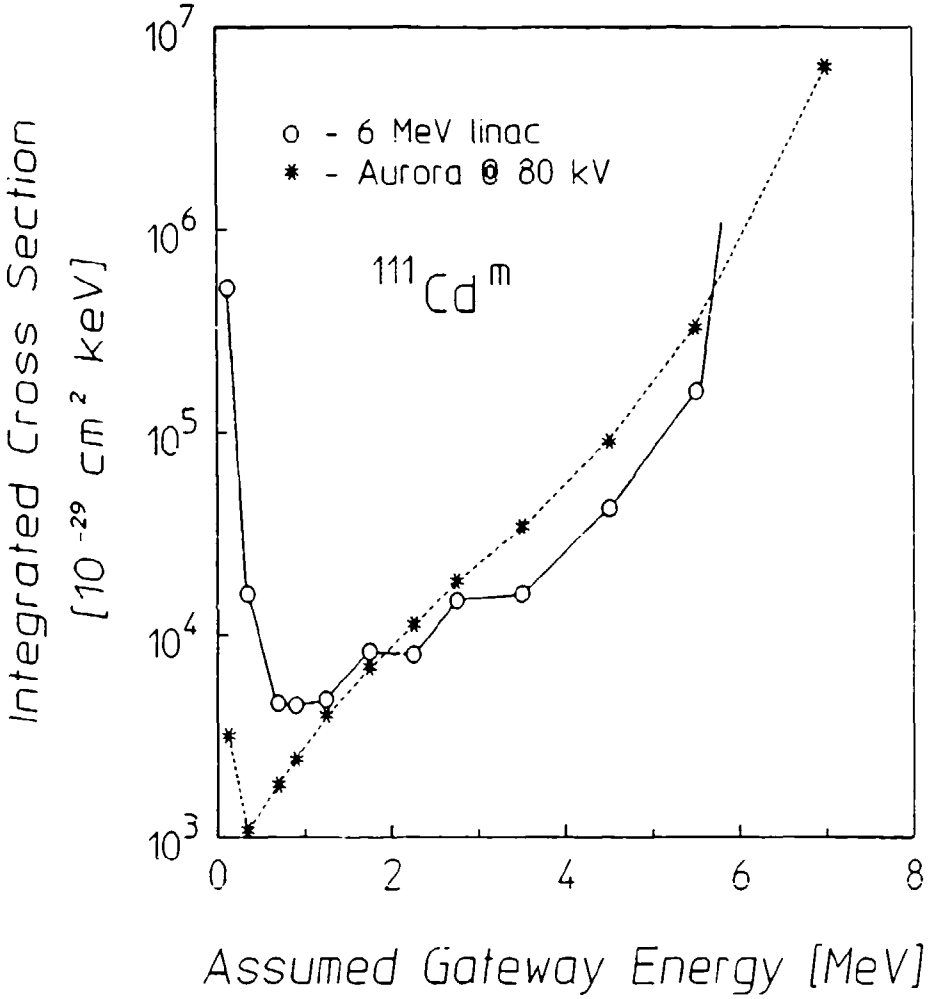

Figure 6: Integrated cross section for a single dominant resonance as a function of the energy at which it is assumed to lie. The circles indicate values derived from previous experimental studies performed with a 6 MeV end-point linac. The asterisks show the results determined from the normalized activation produced by DNA/Aurora when charged to 80 kV.

The second grouping of phenomena includes nuclei for which the normalized activation increases in a smooth and roughly linear manner over the range of energies examined here. This behavior is seen in Figure 7, which presents the results for ^{87}Sr and ^{115}In, two typical examples. Here there is no sign of resonant absorption, but neither is there any clear evidence of a strong non-resonant process. The latter type of excitation, when it takes place, is associated with the absorption of photons by a near continuum of states which lie at reasonably high energies. Since the density of nuclear states rises in a much faster than linear fashion, the slow increase in activation seen for these nuclei seems to preclude the possibility of this as the dominant means of photoexcitation. The lack of this type of absorption is further emphasized in Table II, which lists the ratios of normalized activations detected from 100 kV charge voltages shots to those from 80 kV, an increment of about 2 MeV, and the ratios of 6 MeV linac normalized activations to those from the 4 MeV experiments in reference 19. A comparison of these values shows that in all cases, as higher photon energies are accessed, the rate of increase in activation either remains constant or actually diminishes. This indicates that the rise in excitation for each of these isotopes is simply due to the increasing number of photons available for absorption through gateways below 6 MeV as the irradiating bremsstrahlung end point is raised.

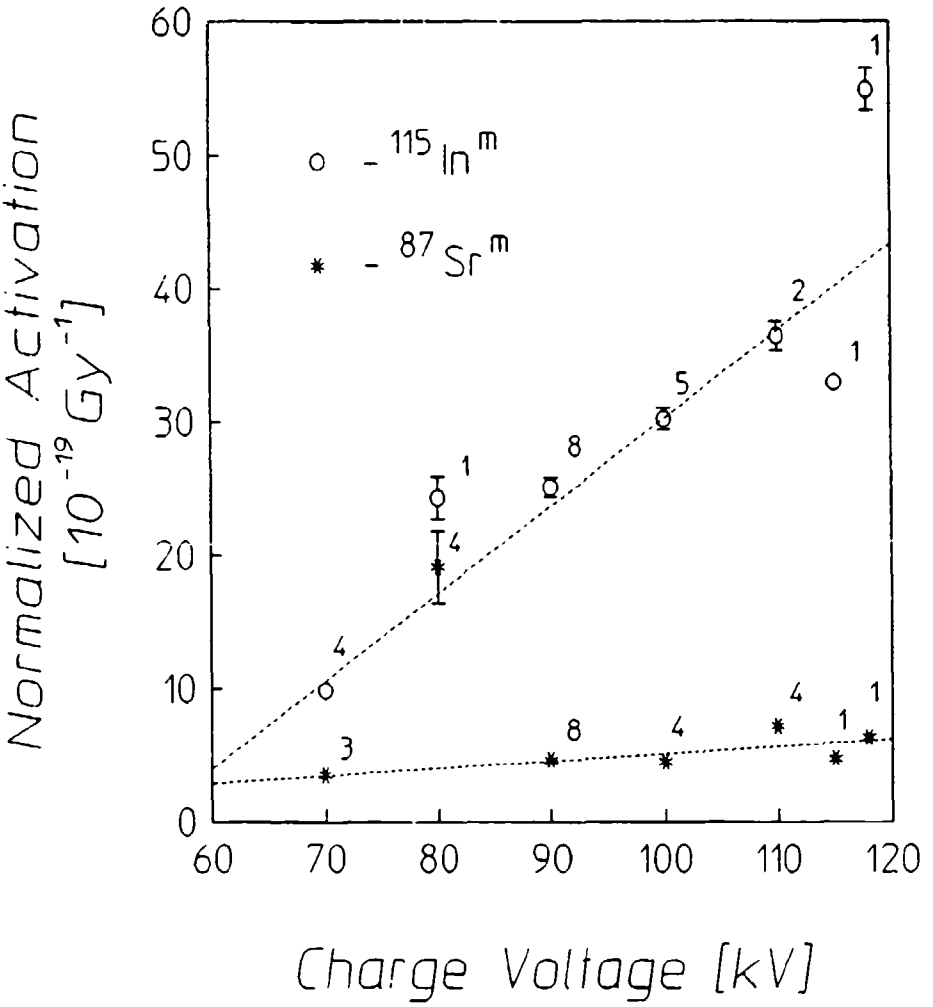

Figure 7: Activation observed in samples containing ^{115}In (circles) or ^{87}Sr (asterisks) following exposure to DX /Aurora shots taken at different charge voltages. These values are the result of multiple measurements as indicated by the numbers to the upper right of the data points. The activation has been normalized to the dosage delivered to the samples. The size of the symbols is comparable to one standard deviation where no error bars are shown.

Table II

Summary of isomeric nuclei which exhibit an essentially monotonic increase in their normalized activation between 70 and 118 kV shots. The quantity A_{100}/A_{80} is ratio of normalized activation resulting from 100 kV shots to that due to 80 kV charge voltages. The values of A_6/A_4 indicate the ratio of the normalized activation achieved following 6 MeV linac irradiations to that from 4 MeV linac exposures.[19]

Isomer	A_6/A_4	A_{100}/A_{80}
$^{79}Br^m$	3.83	1.62
$^{89}Y^m$	32.6	28.0
$^{77}Se^m$	26.8	1.92
$^{137}Ba^m$	7.98	3.04
$^{113}In^m$	4.92	2.33
$^{87}Sr^m$	2.99	1.87
$^{115}In^m$	5.10	2.00
$^{135}Ba^m$	6.53	6.54

The isotopes listed in Table II exhibit similar behavior over the energy range directly observed in the current experiments. However, some important differences appear when the results are examined for information related to gateways lying below 6 MeV. Plots depicting single gateway integrated cross sections contain two interesting features. First, the values derived from the current study for states assumed to lie near 6 MeV are one half to a full order of magnitude larger than the corresponding values obtained from the linac studies. Second, the integrated cross sections obtained from these two experimental series are essentially equal in some range well below 6 MeV. These aspects can be clearly seen in Figure 8 which displays the results for ^{115}In. The relevant question is whether there are any compelling reasons to believe that a true dominant gateway exists and is in some way suggested by this type of plot.

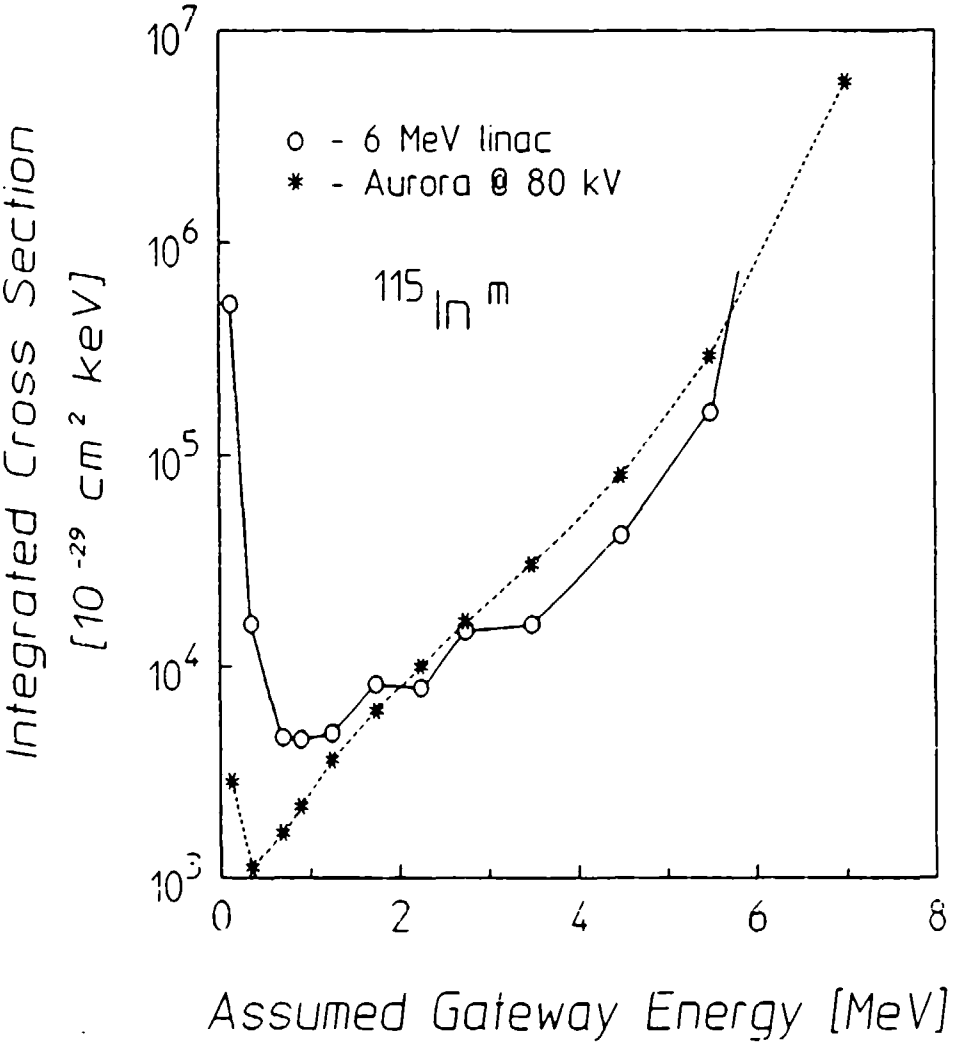

Figure 8: Integrated cross section for a single dominant resonance as a function of the energy at which it is assumed to lie. The circles indicate values derived from previous experimental studies performed with a 6 MeV endpoint linac. The asterisks show the results determined from the normalized activation produced by DNA/Aurora when charged to 80 kV.

The analysis of the experiments of reference 19 supported the position that most of the gateways lying below 6 MeV were in fact somewhere between 1.5 and 4 MeV. It is therefore likely that if one such state is sufficiently large to dominate the photoexcitation up to 11 MeV, plots like that of Figures 4, 6 and 8 will show curves which intersect at the true gateway location below 4 MeV. This appears to be the case for ^{115}In, as well as most of the other nuclei listed in Table II. There is therefore no motivation for believing that the higher integrated cross sections obtained from the current experiments above 5 MeV are truly indicative of an actual state.

There are, however, two exceptions. The isotopes ^{87}Sr and ^{77}Se both exhibit curves which intersect below 1 MeV and whose integrated cross sections from the present study are at least one order of magnitude larger near 6 MeV than those from the previous linac experiments. This is shown in Figure 9 for ^{87}Sr. In this case, as well as for ^{77}Se, it is more probable that dominant gateways are located near 6 MeV rather than at the crossings. This argument is further strengthened for ^{77}Se by the slight downward curvature seen in the normalized activation plot of Figure 10. This shape closely follows that which is intuitively expected for a large resonance near 6 MeV, and lying well below the neutron evaporation threshold at 7.42 MeV. The integrated cross section for this state is on the order of 10^{-23} cm^2-keV. This is fully consistent with the information of Table II which also indicates that the dominant gateway lies between 4 and 6 MeV since the activation ratio changes from 26.8 below 6 MeV to 1.92 above 6 MeV.

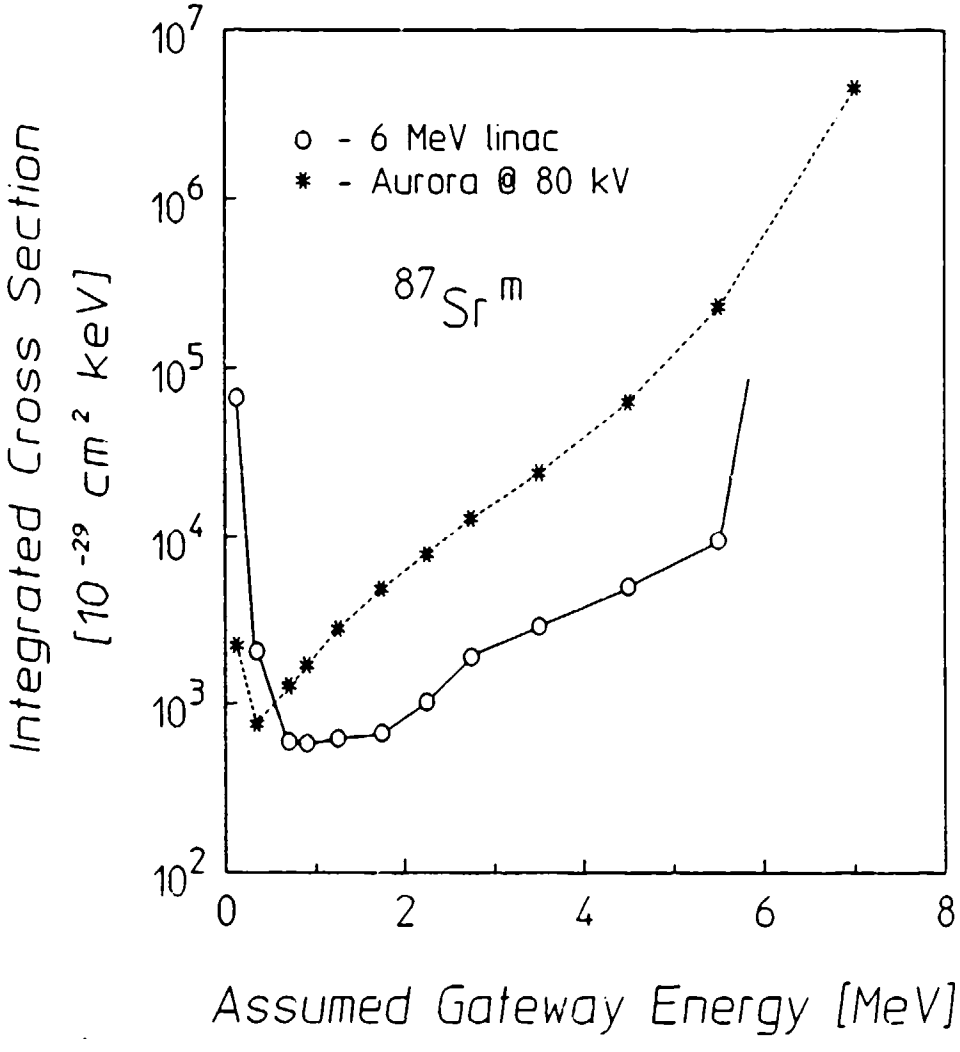

Figure 9: Integrated cross section for a single dominant resonance as a function of the energy at which it is assumed to lie. The circles indicate values derived from previous experimental studies performed with a 6 MeV endpoint linac. The asterisks show the results determined from the normalized activation produced by DNA/Aurora when charged to 80 kV.

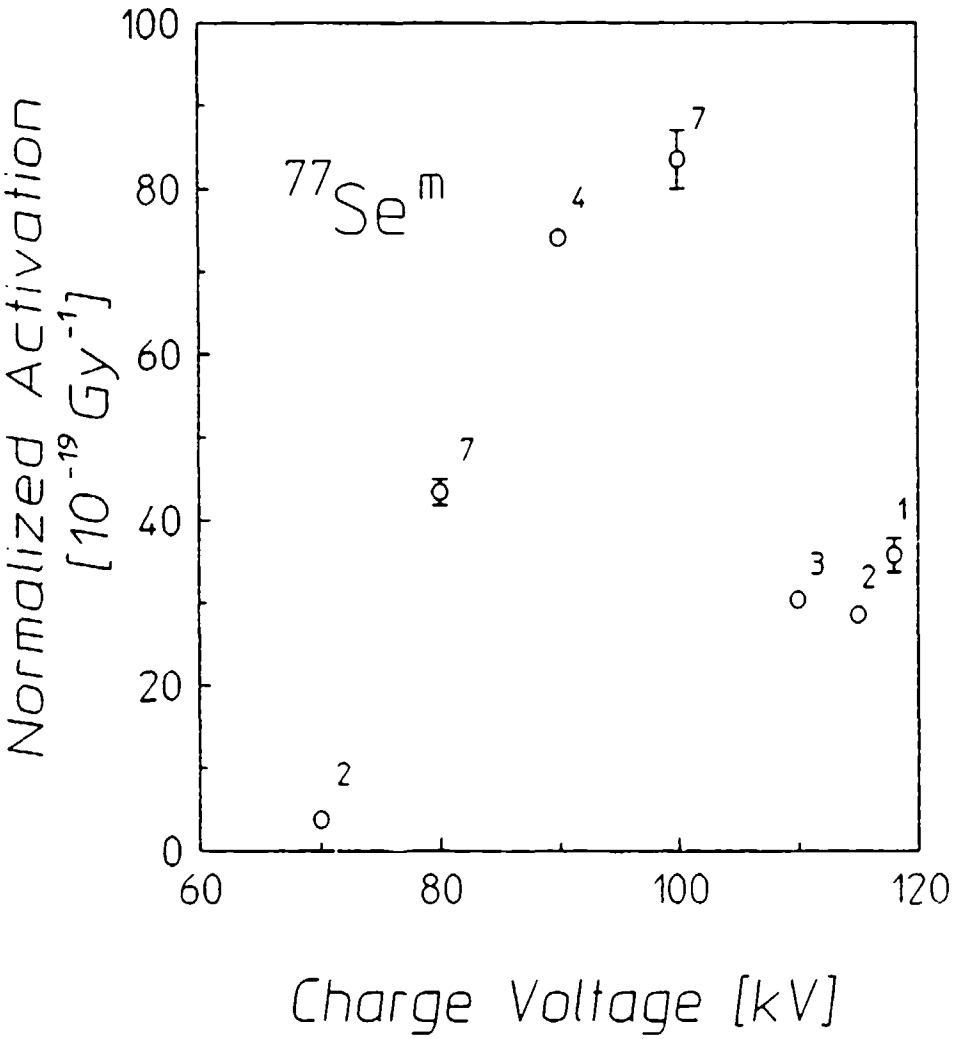

Figure 10: Activation observed in samples containing ^{77}Se following exposure to DNA/Aurora shots taken at different charge voltages. These values are the result of multiple measurements as indicated by the numbers to the upper right of the data points. The activation has been normalized to the dosage delivered to the samples. The size of the symbols is comparable to one standard deviation where no error bars are shown.

Finally, there are three nuclei which cannot at this time be identified with either of the previous classifications. Samples containing these isomers, ^{117}Sn, ^{167}Er and ^{180}Ta, were strongly excited in the current experiments, producing normalized activations on the orders of 10^{-19} Gy^{-1}, 10^{-17} Gy^{-1} and 10^{-12} Gy^{-1}, respectively. However, the small number of measurements taken at only a few charge voltage settings precludes any discussion of the nature of the absorption processes responsible.

Discussion

The observed activations have thus far been examined as being wholly due to photoexcitation through (γ,γ') reactions. However, isomeric populations may also be produced by the interactions of neutrons with the target nuclei through slow neutron capture, or (n,γ), reactions and inelastic fast neutron scattering, or (n,n') reactions. It is important when considering the possibility of neutron contamination of the current results to determine the most probable photoneutron sources in the irradiation environment. The target chamber consists of a large concrete room in which the most intense and high energy photons propagate in an essentially horizontal direction.[22,24] The hot spot where the target samples were placed is centered at about 30 cm from the face of the machine, and is located approximately 1.2 meters above the floor of the 5 meter high chamber. The wall towards which the beam is directed is 19.5 meters away from the sample position. This geometry indicates two factors of importance. First, if fast neutrons are produced by (γ,n) reactions in the intense bremsstrahlung field, the lack of dense moderators near the samples makes it unlikely that a significant thermal or epithermal neutron flux could be present. Second, of the materials within the target chamber only ^{2}H, ^{17}O, ^{13}C, and ^{181}Ta are likely neutron sources since their neutron binding energies are less than the maximum photon energy produced by the accelerator, about 11 MeV. Clearly the most probable source of fast neutrons in the target chamber is the tantalum, with a neutron binding energy of 7.61 MeV. This assumption allows the maximum neutron energies to be found from the estimated endpoint energies of the bremsstrahlung produced at different charge voltages. Table III lists these values.

Table III

Summary of various energy parameters estimated for the charge voltages employed in these experiments. The values given for E_{end} are the approximate endpoint energies of the bremsstrahlung produced by DNA/Aurora. The quantity E_n indicates the maximum possible energy for neutrons produced through (γ,n) reactions.

Charge Voltage [kV]	E_{end} [MeV]	E_n [MeV]
70	6.61	0.00
80	7.56	0.00
90	8.50	0.89
100	9.44	1.83
110	10.39	2.78
115	10.86	3.25
118	11.14	3.53

A determination of the slow neutron flux is made by examining the energy spectra of samples containing natural abundances of the isotopes ^{197}Au and ^{115}In. These nuclei are susceptible to the capture of thermal and epithermal neutrons and produce the daughter nuclei, ^{198}Au and ^{116}In, whose decays are marked by distinct signature lines. The spectra of gold samples show no evidence of full energy peaks above the level of the background at the fluorescence energies of either the ground or isomeric states of ^{198}Au. On the other hand, spectra of indium samples obtained following shots at 100 kV charge voltage do contain very small peaks at the fluorescence energy of 1097.29 keV from the decay of $^{116}In^m$ ($T_{1/2}$ = 54.15 min). The number of counts in these peaks is used to calculate the normalized activation of this species for 100 kV shots and the slow neutron flux which corresponds to this amount of excitation, Φ_{slow} = (168 $\pm$ 31) neutrons/cm^2-Gy. The latter calculation is made by using the thermal neutron cross section rather than the larger epithermal resonance integral.[25] This is done in order to achieve an upper bound on the number of slow neutrons since it is not possible to

determine the proportions of thermal to epithermal neutrons from the targets exposed.

The projected number of slow neutrons produced during a 118 kV shot is found by scaling the 100 kV value by a factor of 1.92 which represents the rise in maximum neutron energy between these charges. The 118 kV shot slow neutron flux is therefore (324 $\pm$ 61) neutrons/cm^2-Gy. The nuclei ^{79}Br, ^{89}Y, ^{113}In, ^{115}In and ^{180}Ta are free from slow neutron contamination since there are no naturally abundant parents for (n,γ) reactions.[26] The largest neutron capture cross section for the production of the remaining isotopes in Table I is 100 barns,[25] the resonance integral for ^{166}Er, and therefore at the highest charge voltage the amount of isomeric activation due to slow neutrons is only 3.24×10^{-20} Gy^{-1}. Thus even in the most critical case, less than 1% of the total activation, on the order of 10^{-17} Gy^{-1}, is provided by slow neutrons.

The number of fast neutrons produced in the target chamber is found in a similar way. Spectra of samples which contained natural abundances of ^{80}Se, ^{82}Se, ^{109}Ag, and ^{116}Cd are examined for any sign of the decay signatures of the daughter nuclei ^{80}As, ^{82}As, ^{109}Pd, and ^{116}Ag which are produced by (n,p) reactions. No such signatures are found above the background level. Nevertheless, it is possible to obtain an upper bound on the numbers of each daughter produced by considering the maximum size of a fluorescence peak which could be hidden by statistical fluctuations of the background. The (n,p) reaction cross sections[27] appropriate to the maximum neutron energies are then used to determine upper bounds on the fast neutron flux. When the scaling of the maximum neutron energies is taken in to account, the most restrictive upper bound is obtained from the reactions ^{80}Se(n,p)^{80}As and ^{82}Se(n,p)^{82}As at 110 kV. The fast neutron flux at this charge is found to be Φ_{Fast} = (209.3 $\pm$ 66.4) neutrons/cm^2-Gy. The number of fast neutrons scaled to 118 kV is then (265.8 $\pm$ 84.3) neutrons/cm^2-Gy. The largest fast neutron cross sections for the elements examined in these experiments are on the order of tens of barns, values much greater than the inelastic cross sections for the particular isotopes in question. The amount of fast neutron activation of these nuclei is therefore on the order of 10^{-21} Gy^{-1}, and again the neutron contamination is found to be negligible.

Conclusion

The current series of experiments serves to examine the process by which nuclear isomers are photoactivated in the previously uncharted energy range from 6 to 11 MeV. The results indicate that even at these energies, photoactivation proceeds through dominant resonant channels. This is both surprising and rewarding since the density of nuclear states is expected to be considerably larger above 6 MeV than at the energies examined in previous experiments.[19] Resonant behavior is demonstrated by the behavior of two nuclides in which a sudden increase or step in the data is due to the presence of a narrow gateway. Two other isotopes support the appearance of large resonances below 6 MeV. Contrasting with this process, several other nuclei show a continuous and roughly monotonic rise in activation which is attributed entirely to contributions from gateways below 6 MeV. Since the earlier studies suggested that the majority of gateways lie below 4 MeV, it appears that the photoexcitation of these nuclear isomers at energies below 11 MeV is dominated by absorption at considerably lower energies. There is no evidence to support the idea of large on-resonant absorption and indeed this is best supported by the failure to activate the heavy nuclei ^{190}Os and ^{192}Os.

The thrust of future experimentation in this field is clearly defined: the energy range from 1.5 to 6 MeV must be scanned by an intense, variable endpoint x-ray source in order to achieve the same degree of success as in the current investigation or in previous studies. A device of this type would allow the specific locations and cross sections for the gateways to be determined. This information would then form the basis of a complete and correct understanding of the photoexcitation of isomeric nuclei at energies below 8 MeV.

Acknowledgment

The assistance, advice and support of the DNA/Aurora facility at the Harry Diamond Laboratories is gratefully acknowledged and in particular F. J. Agee, K. Kerris, G. A. Huttlin and D. A. Whittaker.

References

1. B. Bernstein and I. B. Smith, IEEE Trans. Nucl. Sci. NS-20 (1973) 294.

2. K. G. Kerris, F. J. Agee, D. A. Whittaker, S. G. Gorbics and N. R. Pereira, J. Appl. Phys. 65, 5 (1989).

3. A. Bromborsky et al., Proc. SPIE paper 873-06 (1988).

4. K. G. Kerris in Harry Diamond Laboratories Report No. HDL-TM-81-18, Harry Diamond Laboratories, 1981 (unpublished).

5. B. Pontecorvo and A. Lazard, C. R. Acad. Sci. 208, 99 (1939).

6. G. B. Collins, B. Waldman, E. M. Stubblefield and M. Goldhaber, Phys. Rev. 55, 507 (1939).

7. K. Yoshihara, Zs. Nemeth, L. Lakosi, I. Pavlicsek and A. Veres, Phys. Rev. C 33, 728 (1986).

8. M. Krcmar, A. Ljubicic, K. Pisk, B. Logan and M. Vrtar, Phys. Rev. C 35, 1943 (1987).

9. A. Ljubicic, K. Pisk and B. A. Logan, Phys. Rev. C 23, 2238 (1981).

10. J. A. Anderson and C. B. Collins, Rev. Sci. Instrum. 58, 2157 (1987).

11. J. A. Anderson and C. B. Collins, Rev. Sci. Instrum. 59, 414 (1988).

12. C. B. Collins, J. A. Anderson, Y. Paiss, C. D. Eberhard, R. J. Peterson and W. L. Hodge, Phys. Rev. C 38, 1852 (1988).

13. J. A. Anderson, M. J. Byrd and C. B. Collins, Phys. Rev. C 38, 2838 (1988).

14. M. L. Weidenbeck, Phys. Rev. 67, 92 (1945).

15. E. C. Booth and J. Brownson, Nucl. Phys. A98, 529 (1967).

16. C. B. Collins, C. D. Eberhard, J. W. Glesener and J. A. Anderson, Phys. Rev. C 37, 2267 (1988).

17. A. G. W. Cameron, in *Essays in Nuclear Astrophysics*, edited by C. A. Barnes, D. D. Clayton and D. N. Schramm (Cambridge Univ. Press, Cambridge, 1982), p 23.

18. A. Richter and W. Ziegler, Private Communication.

19. J. J. Carroll, J. A. Anderson, M. J. Byrd, K. N. Taylor, D. G. Richmond, T. W. Sinor, W. L. Hodge, Y. Paiss, C. D. Eberhard, C. B. Collins, E. C. Scarbrough and P. P. Antich, submitted to Phys. Rev. C.

20. J. A. Anderson, C. D. Eberhard, J. F. McCoy, K. N. Taylor, J. J. Carroll, M. J. Byrd and C. B. Collins, in Center for Quantum Electronics Report GRL/8704, University of Texas at Dallas 1988 (unpublished), p 1.

21. *ITS: The Integrated TIGER Series of Coupled Electron/photon Monte Carlo Transport Codes*, J. A. Halbleib and T. A. Mehlhorn, Sandia National Laboratories, SAND84-0573 (1984).

22. *The Aurora Bremsstrahlung Environment*, K. G. Kerris, Harry Diamond Laboratories Report No. HDL-TM-81-18, Harry Diamond Laboratories 1981 (unpublished).

23. "Bremsstrahlung Spectra for University of Texas," by K. G. Kerris, private communication.

24. *Aurora User Guide*, Harry Diamond Laboratories 1987 (unpublished).

25. *Chart of the Nuclides*, Thirteenth Edition, F. W. Walker, D. G. Miller and F. Feiner, Eds. (General Electric Company, San Jose, Calif. 1983).

26. *Nuclear Wallet Cards*, J. K. Tuli (National Nuclear Data Center, Brookhaven National Laboratory, 1985).

27. *Neutron Cross Sections: Volume II, Curves*, Third Edition, D. I. Barber and R. R. Kinsey, BNL 325 (National Neutron Cross Section Center, Brookhaven National Laboratory, Upton, New York, 1976).

N00014-86-C-2488
UTD #24522-964

ADAPTATION OF A FIXED ENDPOINT ELECTRON ACCELERATOR TO PRODUCE VARIABLE ENDPOINT BREMSSTRAHLUNG

by M. J. Byrd, J. J. Carroll, and C. B. Collins

Center for Quantum Electronics, University of Texas at Dallas

Introduction

The study of the photoexcitation of nuclear isomers through (γ,γ') reactions has been underway for more than fifty years[1,2] and has yielded a few interesting results. However, in this time the techniques of nuclear spectroscopy employed in these studies have never reached the level of precision that is associated with the analogous optical methods. Experiments carried out in the latter realm are heavily dependent on the use of intense, monochromatic photon sources which are well-characterized over a tunable range of wavelengths. This type of device is not available for (γ,γ') studies since the energies at which these reactions take place are generally on the order of a few MeV. The lack of such a seemingly vital experimental tool is not due to insufficient technology, but is a consequence of the general properties of matter encountered at these higher energies.

Everything is relatively transparent to the high energy photons necessary for photoexcitation studies. For example, even a heavy element like lead has a mass attenuation coefficient of no more than 0.045 cm^2/gm for 2 MeV x-rays compared to a value of 128 cm^2/gm at 10 keV. This behavior precludes the construction of straightforward devices like x-ray filters or mirrors for use in the MeV range. Also,

the correspondingly small wavelengths make the development of a high energy monochrometer impossible. There are no material lattice spacings which produce dispersion of such x-rays.

Another unavoidable factor regards the conversion of the kinetic energy of electrons to photons. Accelerators which produce nearly monochromatic electron beams of a few MeV are commercially available and it is indeed possible to vary the particle energies in these machines. This can be simply accomplished by changing the accelerating field parameters or by using a variable current electromagnet and a leaded slit to select from the distribution of electron velocities available. The magnet would serve to separate electrons having different velocities, and the slit would allow only particles having the desired energy to exit the device. However, the generation of photons introduces a polychromaticity which cannot be avoided due to the particular physical mechanism which governs this process.

Highly energetic, light, charged particles, such as electrons and positrons, interact with matter through the Coulomb field of the nucleus and outer electrons of atoms within a target. This may be described as the exchange of a single virtual photon between the atomic field and the free particle. Bremsstrahlung is produced when energy is lost in the collision through the emission of a real photon.[3] The x-ray created in this way will have an energy given by the difference between those of the incident and scattered particles. The probability that a particular energy is lost by an electron in this process is given by the Kulenkampff approximation.[4] This distribution is a monotonically decreasing function which reaches zero at the kinetic energy of the incident electron. Therefore, even if only one interaction occurs per particle, as in a thin converter target, a continuous bremsstrahlung spectrum is produced which resembles the Kulenkampff function. In contrast, a thicker target produces a more complex spectrum, since there is an increased possibility of multiple interactions. In general, electrons in the original beam lose some, but not all, of their energy in the primary collisions. If secondary bremsstrahlung events occur, each produces photons according to probability distributions with lower endpoints. The final photon spectrum is therefore the result of a convolution of many Kulenkampff distributions arising from both primary and secondary interactions.

There is obviously no way to avoid the polychromaticity inherent in MeV photon sources. The only recourse left to an experimenter interested in precise (γ,γ') reaction studies is to use a variable x-ray device which produces a continuum distribution of photon energies up to the endpoint. Machines with this property come in many types, ranging from nuclear simulators driven by Marx banks like the DNA/PITHON and DNA/AURORA accelerators, to variable endpoint linacs like that at NRCC, and the superconducting accelerator at the Technische Hochshule Darmstadt. Each of these can be used to uncover important information by exposing samples to bremsstrahlung having different endpoint energies. In this type of study, the energy range of interest is scanned by tuning the source and the amount of photoexcitation observed reflects the processes through which the (γ,γ') reactions proceeded. If resonant absorption of the incident photons at the energy E provides the dominant channel of excitation in a certain isotope, no activation can be measured following exposure to photons having energies less than E. When bremsstrahlung with an endpoint larger than E is used, activation of the sample can be detected. The sharp rise in the amount of excitation as greater endpoint irradiations are used allows the measurement of both the location and the integrated cross section for the state. Conversely, if the photoexcitation proceeds through a non-resonant channel, the activation rises in a continuous and accelerating fashion as the endpoint energy is increased.

Experiments of the above type have been performed and are documented in the literature,[5-13] but their numbers are limited due to the scarcity of these variable endpoint x-ray sources. More numerous are commercial fixed endpoint devices such as medical linacs, and extensive studies have been performed on some nuclides with both 4 and 6 MeV machines.[14-25] However, much of the information gained in this way is inferential since only a limited comparison is possible between the activations observed following the irradiations. It is clear that the complete determination of the nature of (γ,γ') reaction processes requires the in-house development of a tunable bremsstrahlung source capable of energies up to at least 4 MeV.

This report describes the hypothetical modification of a linac having an endpoint fixed at 4 MeV in order to accomplish this goal. The tunability can be achieved by a combination of low Z electron beam moderators and a bending magnet. The important problem of characterizing the output of such a device and guiding further refinements in its

design is solved by extensive use of the Electron Gamma Shower code, EGS,[26] to simulate the complex electron-photon transport.

Design

There are several key requirements which an x-ray source must satisfy in order to be useful for extensive and detailed photoexcitation studies. These are, in the order of their importance:

1) Range of tunability. Previous studies have examined (γ,γ') reactions for photon energies up to about 11 MeV,[13] but a more detailed examination of photoexcitation from 1 to 6 MeV is needed. The device under consideration here must be sufficiently tunable to scan either all of this range, or a large portion thereof.

2) Resolution. Photoexcitation through (γ,γ') reactions proceeds primarily by resonant absorption below 6 MeV.[16] In order to accurately locate the resonances and measure the integrated cross sections of these states, the device must allow good resolution between measurements obtained from different endpoint bremsstrahlung. The maximum allowable step size by which the endpoint may be changed to provide this resolution is chosen to be 0.125 MeV. Of course, an ideal machine would be continuously tunable.

3) Intensity. Previous experiments have shown that, for many isomers, the integrated cross sections for excitation through resonant states below 6 MeV are on the order of 10^{-27} cm^2-keV.[16] Therefore, statistically significant levels of activation can only be reached with a spectral intensity on the order of 10^8 photons/cm^2-keV-sec at the resonance energy.

4) Experimental convenience. The modification of the original accelerator should not preclude other modes of operation. Also, the changeover procedure between modes should be convenient.

These criteria may be met by modifying a fixed endpoint linac similar to commercially available units designed for medical purposes. Figure 1 shows a sketch of the beam head of a treatment linac configured

in the photon mode. A converter target is placed in the path of the electron beam resulting in the production of intense bremsstrahlung. The conversion efficiency from electrons to photons is roughly 100 to 1 when an x-ray target is used. The resulting field is predominantly forward-lobed, particularly at higher energies, so cone shaped filters are centered in the x-ray path to flatten the photon distribution. Collimating jaws are used to confine the region of treatment. As outlined in the introduction, the endpoint energy of a photon distribution may not be changed. Therefore, a machine being adapted for these purposes must be capable of producing an undisturbed electron beam.

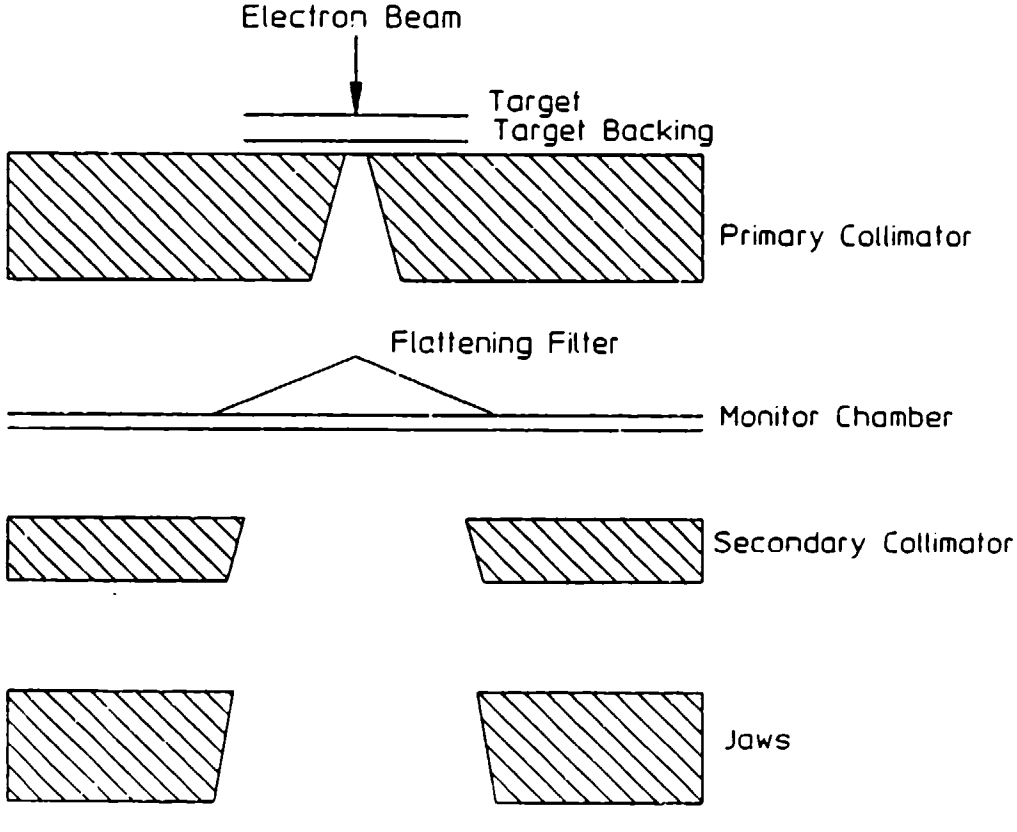

Figure 1: Cutaway view of the beam head of a typical medical treatment linear accelerator operating in the photon mode.[27]

Although there are medical devices available which yield electrons, they do not conform to the prerequisites listed. First, the beam current is reduced by a factor of 100 to bring the electron induced dose down to a level commensurate with that delivered in the photon mode. Also, a thin foil in the beam path serves to spatially spread the electrons without reducing their energies. Both of these actions tend to limit the intensity of any device based on such a source to levels not useful for (γ,γ') studies.

The foremost alteration of the device then is to secure full beam current in the electron mode without a scattering foil. This is simply accomplished by overriding certain interlocks, a perfunctory change to a device not dedicated to medical applications.

The endpoint energy of a bremsstrahlung distribution depends on the maximum energy of electrons impinging on the converter target. Therefore, the tunability requirement may be fulfilled by demanding that the electron endpoint be variable. The most straightforward means of accomplishing this is to use low Z moderators to degrade the endpoint of the electron distribution prior to conversion.

The energy loss of electrons as they pass through matter is dominated by two processes. One of these mechanisms, termed collisional loss, results in an exchange of energy between the incident particle and the target atom, producing either excitation or ionization. The alternative channel is called radiative loss and corresponds to a transfer of energy from an electron to the surrounding electromagnetic field in the form of a real photon. Each of these processes has a corresponding stopping power, or average energy loss per unit pathlength.

When an efficient conversion of electrons to photons is desired, the ratio of radiative to collisional stopping powers should be high. Between 1 and 6 MeV, this ratio is approximately proportional to the atomic number, Z. Therefore, a high Z material is appropriate for the efficient production of bremsstrahlung. Tungsten is the material most often selected for this task.

Conversely, if it is desirable to reduce an electron's energy while minimizing the production of radiation, a low Z material is more

appropriate. In the energy range of interest, the minimum energy loss of an electron passing through such a medium is approximately inversely proportional to the thickness of such a degrader. This is how tunability is achieved in this design. Furthermore, resolution is only restricted by the thinnest increments of degrader material available.

Consider an electron beam incident on a slab of low Z material. Even though the photon flux at the exit plane is very low, the beam on that side is comprised of both photons and electrons. Some of these photons have energies greater than the reduced electron endpoint and are defined as contamination for purposes of this work. A more complex design is therefore necessary in order to separate the degraded electrons from the contaminant photon beam prior to conversion.

Removal of the electrons from the mixed beam is accomplished by applying a magnetic field perpendicular to the beam axis. The magnetic field strength required to bend a 4.0 MeV electron 90 degrees with a radius of curvature of 3.0 cm is 5.0 kG, indicating an electromagnet of very reasonable size. After this bend and some displacement from the converter site, the remaining kinetic energy of the electrons is converted into photons. The geometry is further improved by placing lead collimators between the converter and the sample to be irradiated. Contaminant photons produced at high enough angles to pass through the converter are attenuated by extending the distance between the converter foil and the sample. An overhead view of the final design is shown in Fig. 2, including some simulated electron and photon trajectories.

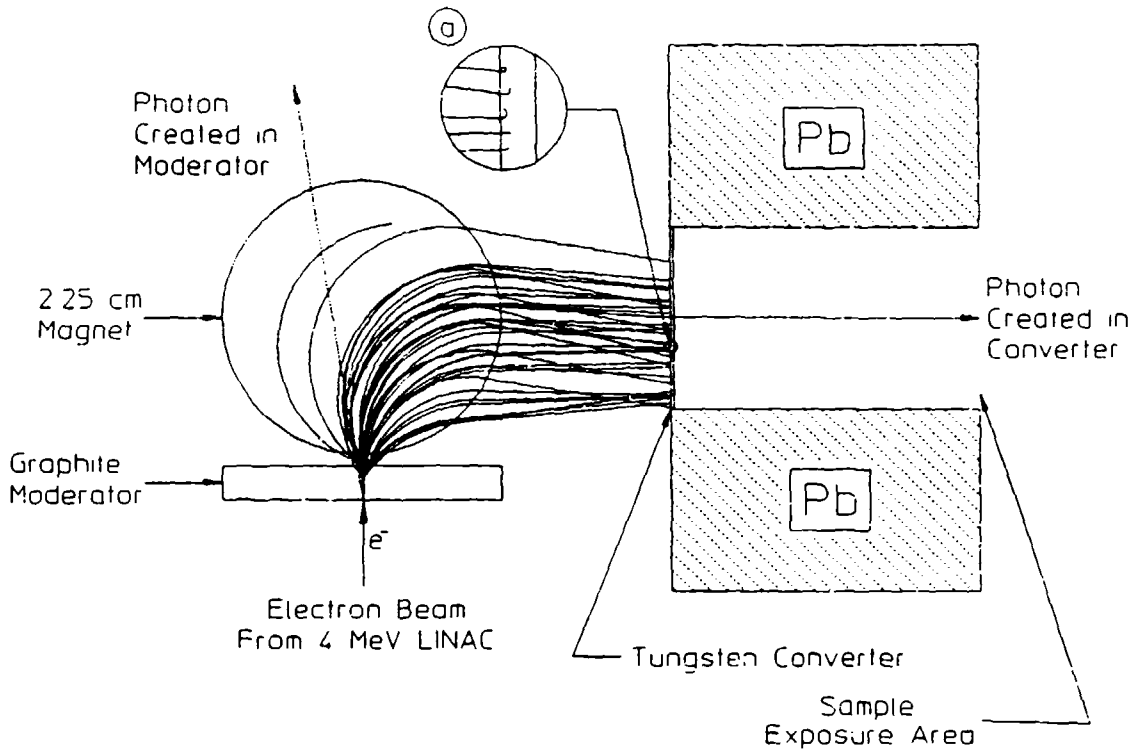

Figure 2: Cross sectional view of variable endpoint bremsstrahlung source. Electron trajectories are shown in solid lines while the dashed lines represent photons. Inset (a) is a closeup of electrons in the converter foil.

This configuration meets the design criteria listed above. However, it is necessary to thoroughly simulate the transport of electrons and photons through all components of this system. These results extend confidence in this design and return quantitative results regarding the actual photon distribution at the sample exposure position.

Simulation Procedures

Most of the computing described here was performed on the Hewlett Packard 9000 Model 560, configured with 4 megabytes of memory and three 32 bit CPU's, each with built-in floating point coprocessors. This computer performed these types of tasks at about 25% the rate of a Convex C1 (CPU time, without implementation of optimizing compiler directives) and at roughly 20 times the rate of an IBM PC/AT with an 80287 math coprocessor.

The coupled electron-photon transport code used is version 4 of the Electron Gamma Shower Code (EGS4), a very general transport program that allows the user to control the initialization, input, output, and geometry checking routines. The actual transport is governed by sophisticated internal electron and photon subroutines. Scattering cross sections, stopping powers, and various other material data are prepared by another program called PEGS (pre-EGS). The PEGS data necessary for this study were generated on a micro-Vax at the University of Texas Southwestern Medical Center.

Earlier versions of EGS were originally intended for higher energy transport than the region of interest here. One artifact of this was carried into version 4 and requires particular attention. Specifically, electron step sizes are too large in the default mode. The authoritative article on the subject[28] suggests the remedy of limiting the step size to correspond to a user defined percentage change in the energy of the electron. The procedure that accomplishes this, FIXTMX, was implemented in all of the simulations. Care was taken, in accordance with Ref. 28, to make sure that multiple scattering was not "turned off" by setting the percentage energy change, ESTEPE, too low. Appropriate cutoff energies for secondary electron production, as defined in Ref. 28, were used to prevent the appearance of spurious artifacts in the photon spectra.

Geometry subroutines and macros are included with the EGS4 distribution tape to assist the user in writing the geometry checking routines. Two of those routines, PLANE1 and CYLNDR, were used extensively. The first of these returns whether or not a plane is intercepted by the current particle trajectory, and if so, the distance to the inter-

section. The second is similar, except that is operates on cylinders centered on the z axis. DNEAR is a global variable in EGS that represents the distance to the nearest boundary crossing. The user can override boundary checking when a particle's shortest distance to a boundary is greater than the current step size by setting this variable. This was implemented in some regions, sometimes with as much as a 25% increase in the rate of calculation.

The prototype moderator was modeled first. Graphite was selected as the degrader because it has a low atomic number, is moderately dense, and is commercially available in thin slabs. Our calculations showed that beryllium might be about 35% more efficient for the degradation of the 4 MeV electrons to those around 2.5 MeV, but unfortunately requires special handling because of its toxicity. Also, the question of neutron evaporation can be avoided altogether by using graphite as the moderator material, since its evaporation threshold is 4.95 MeV (for the ^{13}C isotope) while that of beryllium is 1.67 MeV.[29] The graphite density used for all calculations was 2.0 gm/cm^3.

Figure 3 shows the energy distribution for electrons exiting graphite degraders of varying thicknesses. For each of the distributions shown here, 100,000 incident electrons were input. Figure 4 represents the contamination produced in the degrader, showing the angular distribution of photons with energy above the electron endpoint, as registered immediately on the exit plane of the graphite. The results of 750,000 histories were computed and normalized to the estimated beam current of the LINAC, 25 micro-Amps. Channels corresponding to higher angles registered 0 or 1 counts, indicating a very low likelihood of producing contaminant photons at high angles. This feature is used, along with collimator design, to eliminate the possibility of contamination reaching the sample exposure area.

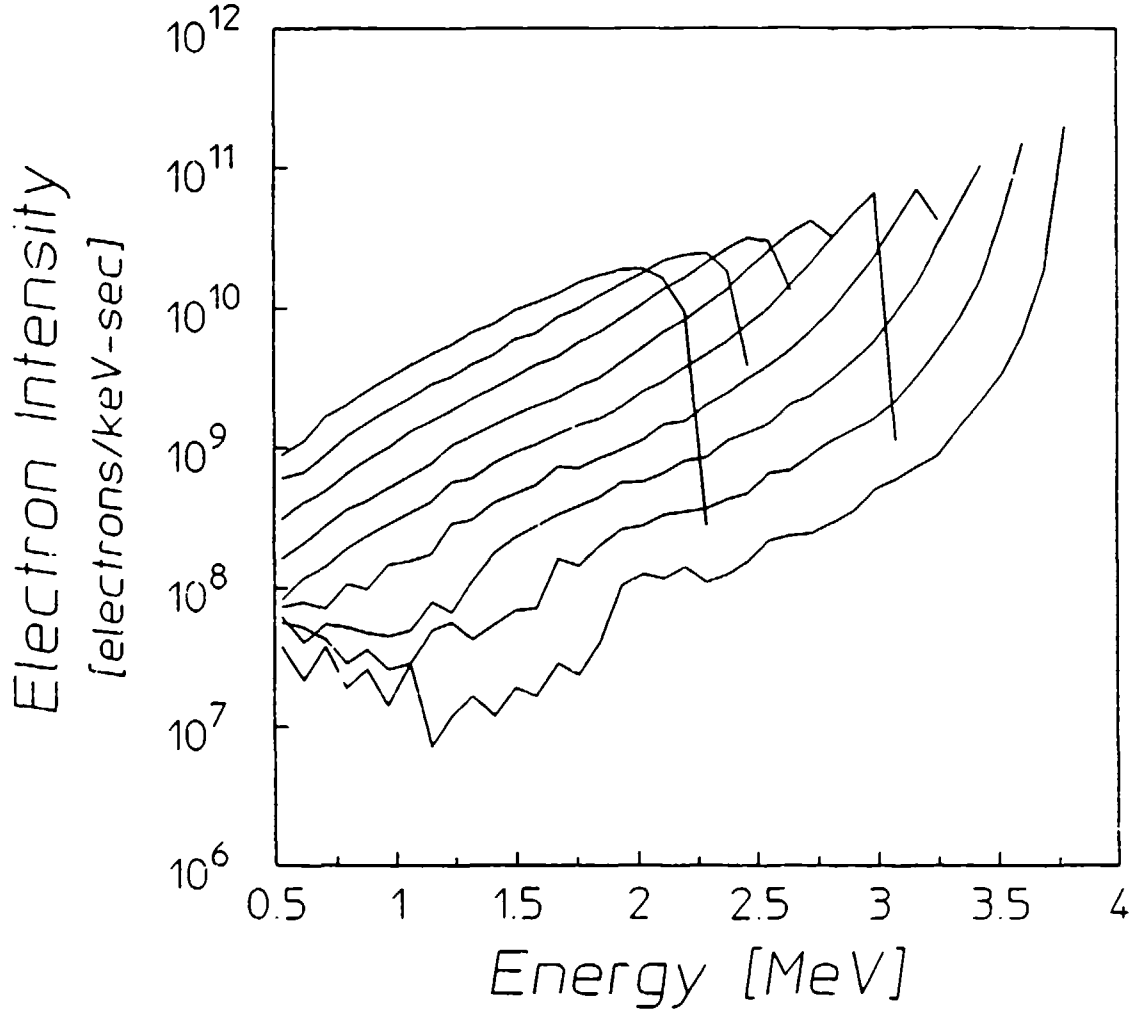

Figure 3: Electron distributions on the exit plane of the degrader slab composed of graphite. Degrader thicknesses vary from 0.07 to 0.63 cm in increments of 0.07 cm. For each curve, 100,000 histories were simulated and the results normalized to a time averaged beam current of 25 μA.

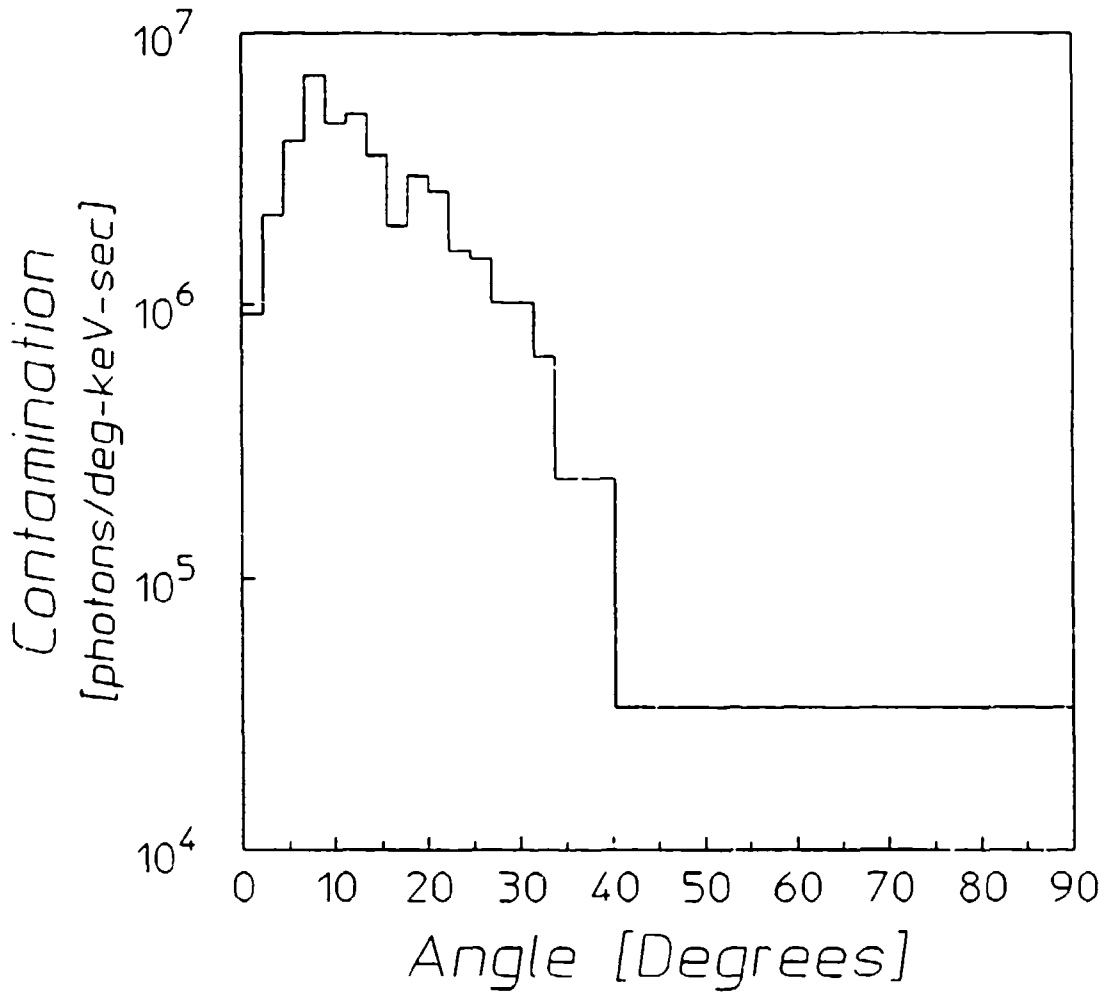

Figure 4: Photons produced in the degrader of energy greater than the electron endpoint. This graph represents the output of 750,000 4 MeV electrons incident on a 0.42 cm slab of graphite, corresponding to an endpoint energy of about 3 MeV. To obtain the same units as Fig. 6, simply divide by 0.11 × r^2, where r is the distance from the point of incidence of the electrons on the moderator to the point of observation.

Other segments of the design were then introduced into the simulation, one region at a time. The first of these was the magnetic transport region. Electrons exiting the degrader were transported through a small air interval to a cylindrical region of constant magnetic field in the negative z direction. Field strengths, typically of about 5 kG, were chosen to optimally bend and focus electrons very close to the end-point energy of the electron distributions shown in

Fig. 3. This favors the high end of the output spectrum for reasons that will become apparent in the following applications section.

The magnetic field region is bounded above and below by magnet pole caps assumed to be composed only of iron. The pole spacing was computed using a quadratic least squares fit to data given by the distributor concerning the maximum attainable field strength for a given pole gap.[30] The gap between the poles was originally presumed to be air-filled, just as in the magnetic field transport problem outlined in the EGS4 manual.[26] The step size required for accurate magnetic field transport, however, was so short that a majority of the simulation time was spent on this region. Most of the electron trajectories in air using the EGS method did not seem to differ much from the paths they would travel in a vacuum. It was therefore decided to model the magnet gap as being a vacuum and to calculate the exit position and direction of the electron based its initial energy, position, and direction (the energy, of course, would remain constant).

Electrons striking the pole pieces in the air-filled gap model were transported until they either exited or fell below the cutoff energy. These electrons did not affect, in most cases, the final output intensity at the sample exposure plane. They did however introduce the possibility of a photon being produced in the magnet pole and passing through the converter to that area. An electron striking the pole in the evacuated gap model was discarded immediately since these do not contribute greatly to the output spectrum. A benchmark case between the two methods is shown in Fig. 5. Note that just below the endpoint energy, the intensity for the vacuum model is consistently about five times that of the air model. The present magnetic field transport subroutine indicates that data acquisition times might be cut by a factor of 5 by the evacuation of the volume the electrons travel through. The difference between the models is probably attributable to the degrading effect of air on the electron energy.

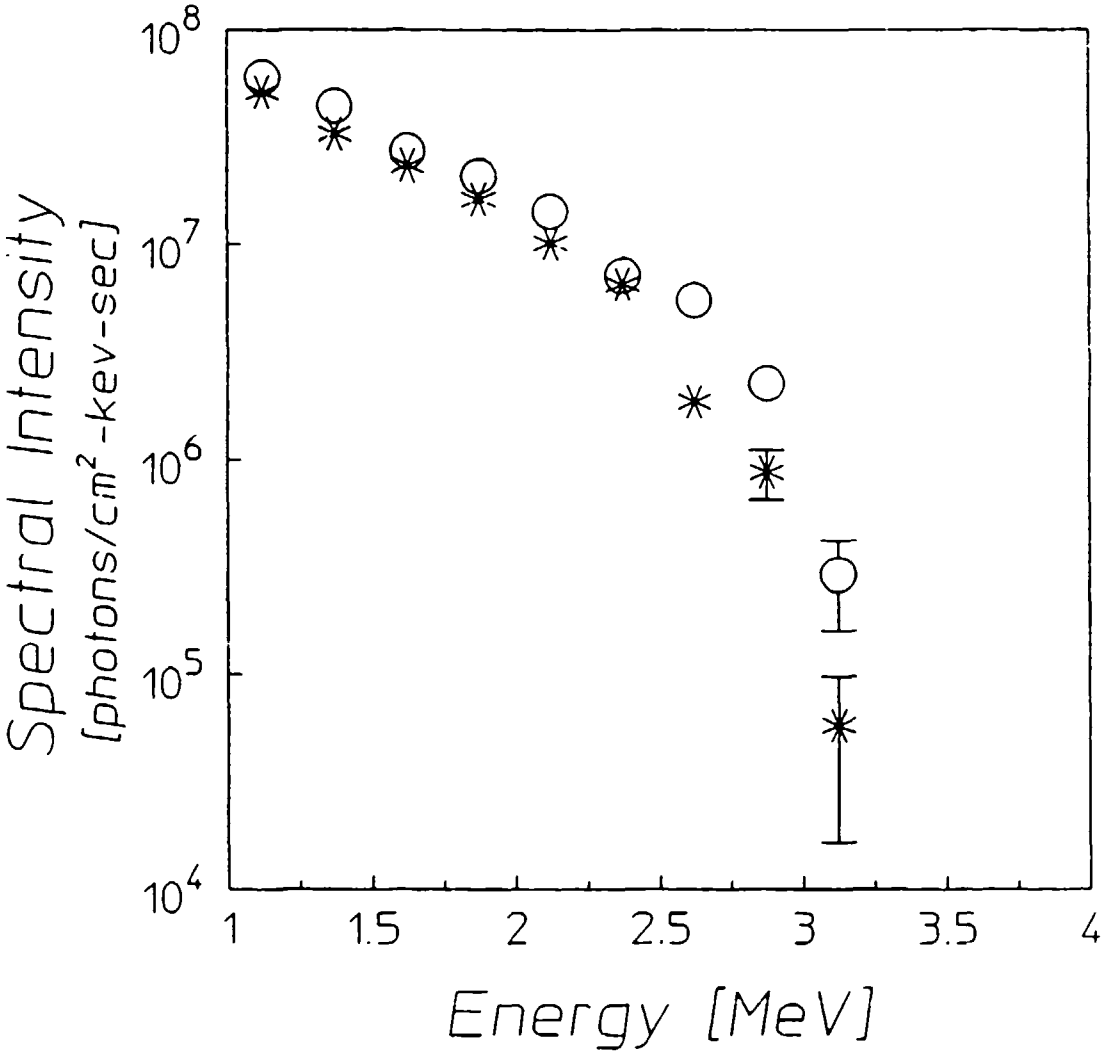

Figure 5: Comparison between air-filled and evacuated models of the magnetic field transport region. The circles represent the results of a vacuum model while the asterisks correspond to the air model spectrum. Where bars are not shown, the uncertainty is bounded by the size of the plotting symbol.

Upon exiting the magnetic field region of the spectrophotometer, most of the electrons impinge upon the tungsten converter, assumed to be 0.056 cm thick. A small percentage of these are converted into photons and travel down a column of air surrounded by lead that serves to

greatly reduced the probability of a contaminant photon reaching the sample exposure area, as mentioned before. For these runs, the distance between the converter and the sample exposure plane was about 5 cm, but should probably be increased in the future to allow for more dispersion of the photons and better protection from contamination. The sample exposure area was a square of 6 cm per side, corresponding to the largest target sample we routinely use for the excitation of isomers. A root-mean-square radius from the center of this area for photons passing through this plane was typically about 1.3 cm, where 2.1 cm corresponds to an exactly even distribution over a circle of radius 3 cm.

Output spectra for several device settings are shown in Fig. 6 and those settings identified in Table I. Finally, to explore the overall efficiency of this device, the results of a 3 MeV endpoint spectrum are compared with the Varian CLINAC 4/100 output obtained from another source,[31] shown graphically in Fig. 7. The 4 MeV spectrum is obtained by correcting the normalized photon distribution by a time-averaged beam current of 25 μA and a sample position 65 cm from the converter foil. These two spectra are very similar up to about 2 MeV, where the contrast between them is ascribed to the difference between their endpoint energies.

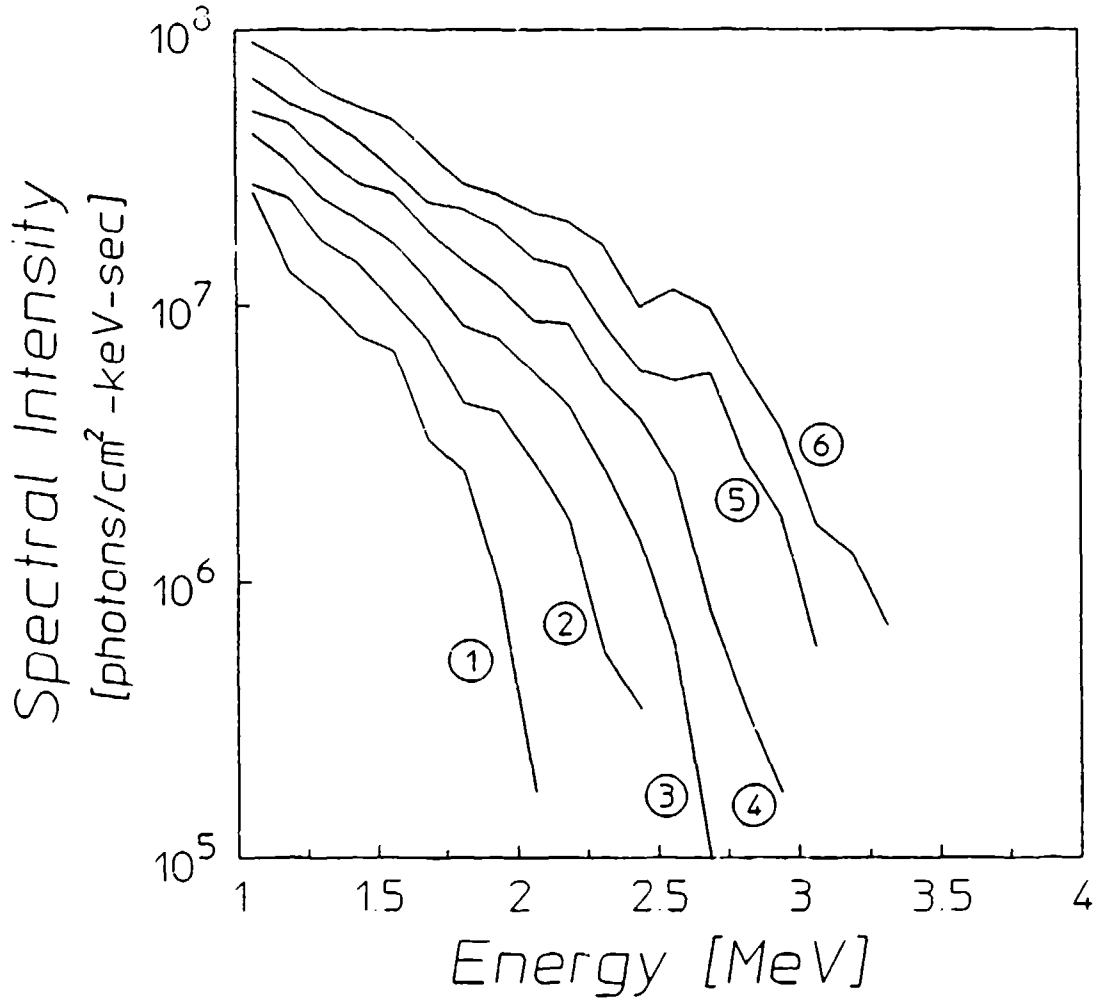

Figure 6: Spectra corresponding to different device settings tuned for varying endpoints. The settings for each spectra are shown in Table I, identified by the circled number next to each curve.

Table I: Summary of spectrophometer settings for spectra of Fig. 6.

Spectrum Number	Thickness of Degrader [cm]	Magnetic Field [kGauss]	Magnet Pole Spacing [cm]	End-Point Energy [MeV]	Histories Run [× 10^5]
1	0.56	3.63	2.58	2.125	4
2	0.49	4.01	2.43	2.500	5
3	0.42	4.38	2.30	2.750	7
4	0.35	4.76	2.17	3.000	4
5	0.28	5.13	2.04	3.125	3
6	0.21	5.50	1.92	3.375	3

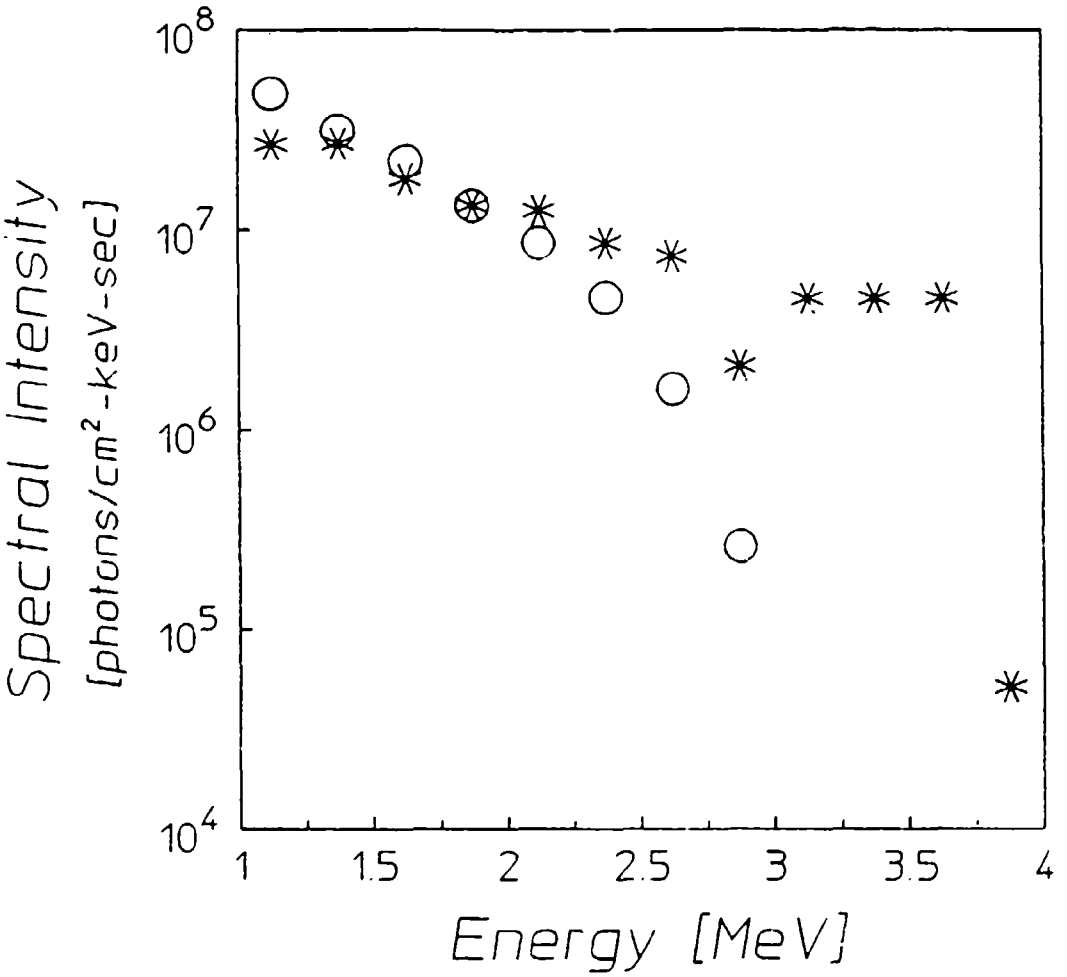

Figure 7: Comparison of 3.0 MeV endpoint results obtained by the design under consideration and CLINAC 4/100 spectrum obtained by using the normalized spectral distribution of Ref. 31 at a distance of 65 cm.

Application - ^{87}Sr

To understand more thoroughly the practicality of this geometry as it relates to (γ,γ') spectroscopy, a test was devised using common experimental parameters. This computational experiment used the isotope most characterized over the energy range of interest[32], ^{87}Sr. The goals of this exercise were to confirm that reasonable exposure

times could be expected and to obtain an upper limit on the width of the energy range in which a state of moderate cross section can be identified.

Some background concerning (γ,γ') reactions is required to understand the implications of tne results of this conceptual experiment. After exposure of an isotope to certain radiation, activation of a metastable level may be observed. Since the transition between the ground and the metastable states is highly forbidden, this photoexcitation must take place through a higher lying intermediary state, sometimes called a gateway state. These states are narrow relative to the spectra of any available sources.

For a continuous source like a linac, the activation rate, or fractional number of nuclei activated per unit time, is related to the integrated cross section by

$$\frac{N_{excited}}{N_T} = \sum_i (\sigma\Gamma)_i \left(\frac{d\Phi}{dE}\right)_i , \qquad (1)$$

where $(\sigma\Gamma)_i$ is the integrated cross section of the i^{th} resonant excitation channel and $(d\Phi/dE)_i$ is the spectral intensity rate in photons/(cm^2-keV-sec) at the sample position and at the i^{th} resonance location. $N_{excited}$ is the number of excited nuclei and N_T represents the total number of nuclei. Experimentally the activation rate is given by

$$\frac{N_{excited}}{N_T} = \frac{C}{D\eta A f T_{irr}} , \qquad (2)$$

where C is the number of counts registered in a full energy fluorescence peak by a detector of efficiency η, D is the finite count time correction, and f is the quantum efficiency associated with fluorescent decay from the metastable state to the ground state. The exposure time is T_{irr} and A is the self absorption correction coefficient.

The pertinent values for the three gateway states identified in Ref. 32 are shown in Table II. These were used, in conjunction with the spectra of Fig. 6, to calculate the expected activation which could be observed for each endpoint. The number of peak counts corresponding to these activations were then computed using the reasonable experimental parameters given in Table III. A Poisson deviate was then taken of this number of counts to simulate random decay results.

Table II: Locations and magnitudes of gateways identified in ^{87}Sr by Booth and Brownson.[32]

Energy [MeV]	Integrated Cross Section [10^{-29} cm^2-keV]
1.22	8.5
1.88	16.0
2.66	380.0

Table III: Experimental parameters used to project the number of counts observed in a 3X3 NaI detector caused by the activation of ^{87}Sr.

Halflife	2.8 h
Irradiation Time	2.0 h
Travel Time	10.0 m
Count Time	1.0 h
Fluorescence Energy	388.4 keV
Gamma Intensity	82.3 %
Self Absorption	3.2 %
Detector Efficiency	3.4 %

From the results of the computer experiment, the activation was then derived back from this skewed number of counts with the parameters of Table III, as though there was no prior knowledge of either the locations or the integrated cross sections for any gateways. Figure 7 shows this randomly deviated activation as a function of the endpoint energy of the x-ray source. From the figure, a sharp rise in activation between 2.5 and 2.75 MeV can be clearly observed, indicating that a gateway of this size is readily measurable. A discussion of more sensitive methods of measuring the exact locations and cross sections of the gateways lies outside the scope of this computational effort.

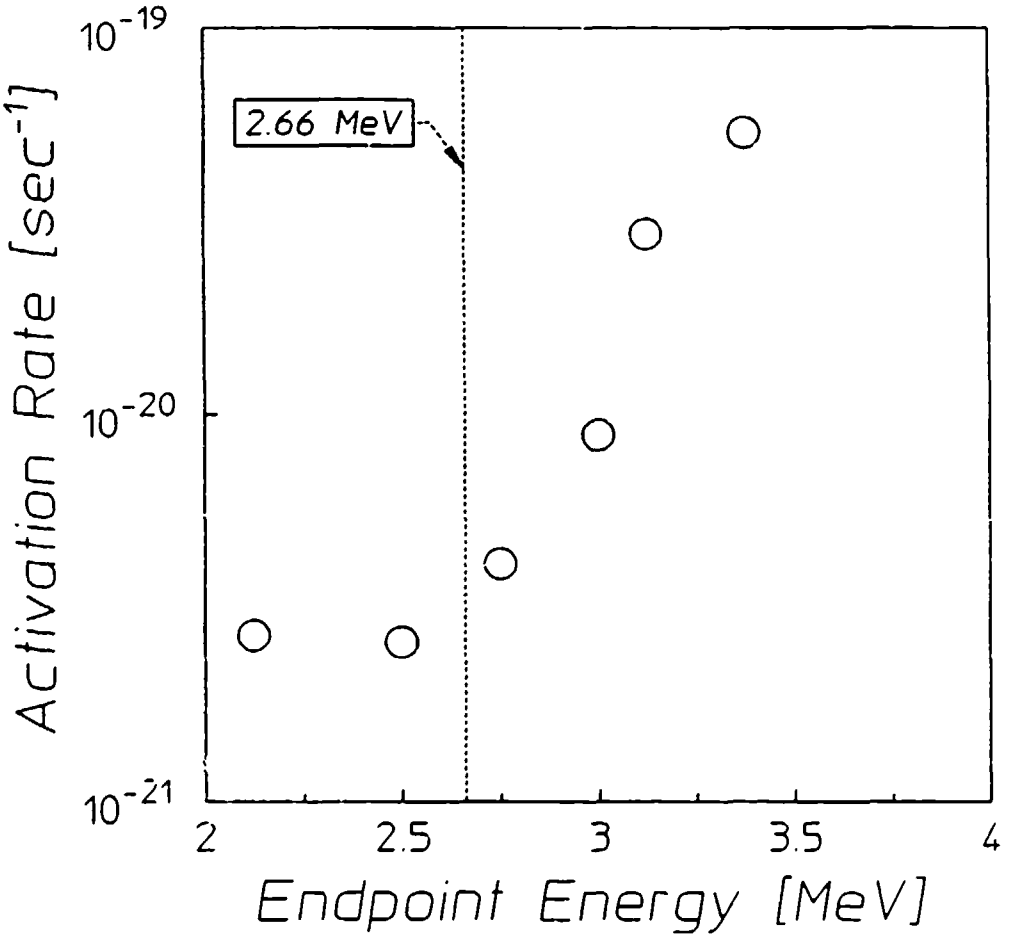

Figure 8: Activation rate due to hypothetical 2 hour exposures of ^{87}Sr to the variable endpoint bremsstrahlung source for each of the endpoints of Table I. The vertical dashed line denotes the position of the 380 unit gateway at 2.66 MeV, where a unit is defined as 10^{-29} cm^2-keV.

Conclusion

The viability has been demonstrated of economically and effectively converting a fixed endpoint electron linear accelerator into a variable endpoint photon source using simple materials and equipment such as graphite, tungsten, lead, and an electromagnet for bending the beam. Furthermore, the proposed modification meets the criteria of tunability, resolution, intensity, and experimental convenience required for such a source to be useful in (γ,γ') studies.

The test case of ^{87}Sr has shown that, for integrated cross sections of about 400 units, the device can serve to locate the energies of the gateway states. For these and the much larger cross sections already observed below 4 MeV,[23] statistically significant results can be expected with very reasonable data acquisition times.

Computational resolution can be improved further by the implementation of the EGS code system on more sophisticated machines than the one currently used. One such computer is the Cray available through the University of Texas Center for High Performance Computing on which microtasking may be exploited. This involves placing a compiler directive before a loop that then feeds the interior of that loop to a large number of processors. Each processor then runs a copy of the code independently and the results are added at the end of the cycle. Monte Carlo methods can benefit tremendously from such microtasking if proper steps are taken to ensure that randomness is maintained between the processors and that the results are added correctly.

Precision will also be improved by advances expected with the release of EGS version 5, expected in the Fall of 1989.[33] In the low energy ranges of interest here, this new code should run about 3-6 times faster and with greater accuracy than the version presently available to us.[34] It will also allow the cutoff energy to be increased, improving the statistical certainty at high energies while maintaining reasonable run times. Nevertheless, all of the anticipated improvements represent refinements which cannot affect the basic results reported here. The adaptation of a fixed endpoint linear accelerator for the production of variable endpoint bremsstrahlung is an attractive and cost-effective option.

References

1. B. Pontecorvo and A. Lazard, C. R. Acad. Sci. 208, 99 (1939).

2. G. B. Collins, B. Waldman, E. M. Stubblefield and M. Goldhaber, Phys. Rev. 55, 507 (1939).

3. S. M. Seltzer, "Cross Sections for Bremsstrahlung Production and Electron-Impact Ionization," in *Monte Carlo Transport of Electrons and Photons*, Ed. T. M. Jenkins, New York: Plenum Press 1988.

4. E. U. Condon, in *Handbook of Physics*, Ed. E. U. Condon and H. Odishaw, New York: McGraw-Hill 1967.

5. J. A. Anderson and C. B. Collins, Center for Quantum Electronics Report #GRL/8602, University of Texas at Dallas, 1987 (unpublished) pp. 29-46.

6. Center for Quantum Electronics Report #GRL/8603, University of Texas at Dallas, 1987 (unpublished) pp. 31-43.

7. C. B. Collins, J. A. Anderson, Y. Paiss, C. D. Eberhard, R. J. Peterson, and W. L. Hodge, Center for Quantum Electronics Report #GRL/8702, University of Texas at Dallas, 1987 (unpublished) pp. 45-56.

8. C. B. Collins, J. A. Anderson, Y. Paiss, C. D. Eberhard, R. J. Peterson, and W. L. Hodge, Phys. Rev. C 38, 1852 (1988).

9. J. A. Anderson, M. J. Byrd, and C. B. Collins, Center for Quantum Electronics Report #GRL/8702, University of Texas at Dallas, 1987 (unpublished) pp. 57-70.

10. J. A. Anderson, M. J. Byrd, and C. B. Collins, Phys. Rev. C 38, 2838 (1988).

11. J. A. Anderson, K. N. Taylor, J. M. Carroll, J. F. McCoy, J. J. Carroll, M. J. Byrd, and C. B. Collins, Center for Quantum Electronics Report #GRL/8704, University of Texas at Dallas, 1988, pp. 36-54.

12. C. D. Eberhard, J. A. Anderson, M. J. Byrd, J. J. Carroll, and C. B. Collins, Center for Quantum Electronics Report #GRL/8801, University of Texas at Dallas, 1988, pp. 15-41.

13. J. J. Carroll, J. A. Anderson, M. J. Byrd, K. N. Taylor, D. G. Richmond, T. W. Sinor, and C. B. Collins, Center for Quantum Electronics Report #GRL/8901, University of Texas at Dallas, 1989, pp. 1-31.

14. C. D. Eberhard, J. W. Glesener, Y. Paiss, J. A. Anderson, C. B. Collins, W. L. Hodge, E. C. Scarbrough, and P. P. Antich, Center for Quantum Electronics Report #GRL/8702, University of Texas at Dallas, 1987, pp. 89-103.

15. C. B. Collins, C. D. Eberhard, J. W. Glesener, and J. A. Anderson, Phys. Rev. C 37, 2267 (1988).

16. J. J. Carroll, J. A. Anderson, M. J. Byrd, K. N. Taylor, D. G. Richmond, T. W. Sinor, W. L. Hodge, Y. Paiss, C. D. Eberhard, C. B. Collins, E. C. Scarbrough, and P. P. Antich, Phys. Rev. C (pending).

17. C. B. Collins, C. D. Eberhard, J. W. Glesener, and J. A. Anderson, Center for Quantum Electronics Report #GRL/8703, University of Texas at Dallas, 1988, pp. 21-28.

18. J. W. Glesener, C. D. Eberhard, and C. B. Collins, Center for Quantum Electronics Report #GRL/8703, University of Texas at Dallas, 1988, pp. 29-35.

19. C. B. Collins, J. A. Anderson, C. D. Eberhard, J. F. McCoy, and J. J. Carroll, Center for Quantum Electronics Report #GRL/8703, University of Texas at Dallas, 1988, pp. 37-56.

20. J. A. Anderson, C. D. Eberhard, J. F. McCoy, K. N. Taylor, J. J. Carroll, M. J. Byrd, and C. B. Collins, Center for Quantum Electronics Report #GRL/8704, University of Texas at Dallas, 1988, pp. 11-35.

21. J. A. Anderson, K. N. Taylor, J. J. Carroll, M. J. Byrd, and C. B. Collins, Center for Quantum Electronics Report #GRL/8803, University of Texas at Dallas, 1988, pp. 1-17.

22. J. J. Carroll, J. A. Anderson, J. W. Glesener, C. D. Eberhard, and C. B. Collins, Center for Quantum Electronics Report #GRL/8803, University of Texas at Dallas, 1988, pp. 19-36.

23. J. J. Carroll, J. A. Anderson, M. J. Byrd, K. N. Taylor, D. G. Richmond, T. W. Sinor, W. L. Hodge, Y. Paiss, C. D. Eberhard, and C. B. Collins, Center for Quantum Electronics Report #GRL/8804, University of Texas at Dallas, 1989, pp. 1-29.

24. J. A. Anderson, C. D. Eberhard, M. J. Byrd, J. J. Carroll, C. B. Collins, E. C. Scarbrough, and P. P. Antich, Nucl. Instrum. Methods in Physics Research, Proceedings of the Tenth International Conference on the Application of Accelerators in Research and Industry, ed. J. L. Duggan and I. L. Morgan, (North Holland, Amsterdam, 1989) pp. 452-454.

25. J. J. Carroll, J. A. Anderson, J. W. Glesener, C. D. Eberhard, and C. B. Collins, Astrophys. J. (pending).

26. *The EGS Code System*, Walter R. Nelson, Hideo Hirayama, and David W. O. Rogers, SLAC Report 265, (Stanford Linear Accelerator Center, Stanford Calif. 1985).

27. R. Mohan, "Monte Carlo Simulation of Radiation Treatment Machine Heads," in *Monte Carlo Transport of Electrons and Photons*, Ed. T. M. Jenkins, New York: Plenum Press (1987).

28. D. W. O. Rogers, Nucl. Inst. and Meth. in Phys. Res. 227, 535 (1984).

29. M. D. Goldberg and J. A. Harvey, "Neutrons," in *American Institute of Physics Handbook*, Ed. D. E. Gray, New York: McGraw-Hill, 1972.

30. GMW Associates, Ian Walker, Private communication.

31. R. Mohan, C. Chui and L. Lidofsky, Med. Phys. 12, 595 (1985).

32. E. C. Booth and J. Brownson, Nucl. Phys. A98, 529 (1967).

33. D. W. O. Rogers, Private communication.

34. A. F. Bialajew, D. W. Rogers, "Electron Step-Size Artefacts and PRESTA," in *Monte Carlo Transport of Electrons and Photons*, Ed. T. M. Jenkins, New York: Plenum Press (1987).

Center for Quantum Electronics
The University of Texas at Dallas
P.O. Box 830688, MS NB11
Richardson, Texas 75083-0688
(214) 690-2863